Lack of APP and APLP2 in GABAergic Forebrain Neurons Impairs Synaptic Plasticity and Cognition

Mehr, Annika ; Hick, Meike ; Ludewig, Susann ; Müller, Michaela ; Herrmann, Ulrike ; von Engelhardt, Jakob ; Wolfer, David P ; Korte, Martin ; Müller, Ulrike C

Abstract: Amyloid- precursor protein (APP) is central to the pathogenesis of Alzheimer's disease, yet its physiological functions remain incompletely understood. Previous studies had indicated important synaptic functions of APP and the closely related homologue APLP2 in excitatory forebrain neurons for spine density, synaptic plasticity, and behavior. Here, we show that APP is also widely expressed in several interneuron subtypes, both in hippocampus and cortex. To address the functional role of APP in inhibitory neurons, we generated mice with a conditional APP/APLP2 double knockout (cDKO) in GABAergic forebrain neurons using DlxCre mice. These DlxCre cDKO mice exhibit cognitive deficits in hippocampus-dependent spatial learning and memory tasks, as well as impairments in species-typic nesting and burrowing behaviors. Deficits at the behavioral level were associated with altered neuronal morphology and synaptic plasticity Long-Term Potentiation (LTP). Impaired basal synaptic transmission at the Schafer collateral/CA1 pathway, which was associated with altered compound excitatory/inhibitory synaptic currents and reduced action potential firing of CA1 pyramidal cells, points to a disrupted excitation/inhibition balance in DlxCre cDKOs. Together, these impairments may lead to hippocampal dysfunction. Collectively, our data reveal a crucial role of APP family proteins in inhibitory interneurons to maintain functional network activity.

DOI: https://doi.org/10.1093/cercor/bhaa025

OXFORD UNIVERSITY PRESS | Cerebral Cortex

Lack of APP and APLP2 in GABAergic forebrain neurons impairs synaptic plasticity and cognition

Journal:	*Cerebral Cortex*
Manuscript ID	CerCor-2019-00596.R1
Manuscript Type:	Original Article
Date Submitted by the Author:	n/a
Complete List of Authors:	Mehr, Annika; Ruprecht Karls Universitat Heidelberg, Institute for Pharmacy and Molecular Biotechnology, Department Functional Genomics Hick, Meike; Goethe University Frankfurt Faculty 16 Medicine, Institute of Clinical Neuroanatomy Ludewig, Susann; TU Braunschweig, Zoological Institute Braunschweig Müller, Michaela; Johannes Gutenberg Universität Mainz Klinikum, Institut für Pathophysiologie Herrmann, Ulrike; TU Braunschweig, Zoological Institute von Engelhardt, Jakob; Johannes Gutenberg Universität Mainz Klinikum, Institut für Pathophysiologie Wolfer, David; University of Zurich, Institute of Anatomy Korte, Martin; TU Braunschweig, Zoological Institute Müller, Ulrike; Ruprecht Karls Universitat Heidelberg, Institute for Pharmacy and Molecular Biotechnology, Department Functional Genomics
Keywords:	Amyloid precursor protein, interneurons, excitation/inhibition balance, behaviour, synaptic plasticity

Lack of APP and APLP2 in GABAergic forebrain neurons impairs synaptic plasticity and cognition

Annika Mehr[1], Meike Hick[1,2], Susann Ludewig[3,4], Michaela Müller[5], Ulrike Herrmann[3], Jakob von Engelhardt[5], David P. Wolfer[6,7], Martin Korte[3,4], Ulrike C. Müller[1]

[1]University of Heidelberg, IPMB, Functional Genomics, Heidelberg, Germany

[2]J.W. Goethe-Universität, Anatomie I - Klinische Neuroanatomie, Frankfurt am Main, Germany

[3]TU Braunschweig, Institut für Zoologie, Zelluläre Neurobiologie, Braunschweig, Germany

[4]Helmholtz Centre for Infection Research, Neuroinflammation and Neurodegeneration Group, Braunschweig, Germany

[5]Universitätsmedizin Mainz, Germany

[6]University of Zürich, Institute of Anatomy, Zürich, Switzerland

[7]Institute of Human Movement Sciences and Sport, ETH Zürich, Zürich, Switzerland

Corresponding author:

Ulrike Müller

Im Neuenheimer Feld 364, R511

69120 Heidelberg

Phone: +49 6221 54 6717

Facsimile number: +49 6221 54 5830

Email: u.mueller@urz.uni-heidelberg.de

Running title: APP/APLP2 knockout in GABAergic neurons

Abstract

Amyloid-β precursor protein (APP) is central to the pathogenesis of Alzheimer's disease (AD), yet its physiological functions remain incompletely understood. Previous studies had indicated important synaptic functions of APP and the closely related homologue APLP2 in excitatory forebrain neurons for spine density, synaptic plasticity, and behavior. Here, we show that APP is also widely expressed in several interneuron subtypes, both in hippocampus and cortex. To address the functional role of APP in inhibitory neurons we generated mice with a conditional APP/APLP2 double knockout in GABAergic forebrain neurons using DlxCre mice. These DlxCre cDKO mice exhibit cognitive deficits in hippocampus-dependent spatial learning and memory tasks, as well as impairments in species typic nesting and burrowing behaviors. Deficits at the behavioral level were associated with altered neuronal morphology and synaptic plasticity (LTP). Impaired basal synaptic transmission at the Schafer collateral/CA1 pathway that was associated with altered compound excitatory/inhibitory synaptic currents and reduced action potential firing of CA1 pyramidal cells point to a disrupted excitation/inhibition (E/I) balance in DlxCre cDKOs. Together, these impairments may lead to hippocampal dysfunction. Collectively, our data reveal a crucial role of APP family proteins in inhibitory interneurons to maintain functional network activity.

Words 193, allowed 200

Key words

Amyloid precursor protein, interneurons, excitation/inhibition balance, behaviour, synaptic plasticity.

Introduction

Synaptic dysfunction and synapse loss are key features of Alzheimer's pathogenesis that occur at early stages of AD, while deposition of the β-amyloid (Aβ) peptide in extracellular plaques, a major hallmark of AD, develops only at later stages of AD (Terry RD et al. 1991; Selkoe DJ 2002). Aβ is generated by sequential β- and γ-secretase processing of APP. To date, extensive biochemical and genetic studies, including those involving numerous APP transgenic mice have mainly focused on the role of Aβ for AD pathogenesis. Despite this, our understanding of AD pathogenesis is still incomplete and all Aβ centered treatment approaches, including Aβ immunotherapy and secretase inhibitors have failed so far (Yang, R 2019). In contrast, much less is known about the physiological role of APP and the related APLPs for neuronal, synaptic and network functions that involve different neuronal cell types. A still unresolved question is whether loss of synaptic APP functions in excitatory or inhibitory cell types might contribute to AD.

APP belongs to a small gene family comprising in addition APP like protein 1 and 2 (APLP1 and APLP2). APP and APLP2 show a similar structural organization and widespread expression throughout the brain, which is particularly high in pyramidal cells of the cortex and hippocampus (Hick M et al. 2015; Del Turco D et al. 2016; Richter MC et al. 2018). APP and APLP2 have been shown to localize to synaptic sites (Schilling S et al. 2017), including the presynaptic active zone (Lassek M et al. 2013; Wilhelm BG et al. 2014). Major insights into the physiological functions of APP and the related APLPs were obtained from knockout models (Mockett BG et al. 2017; Müller UC et al. 2017). Studies using constitutive APP-KO mice indicated that APP plays a crucial role for the formation, maintenance, turnover, and plasticity of synapses, including long-term potentiation (LTP) (Dawson GR et al. 1999; Seabrook GR et al. 1999; Ring S et al. 2007; Weyer SW et al. 2011; Tyan SH et al. 2012; Weyer SW et al. 2014; Ludewig S and M Korte 2016; Zou C et al. 2016; Hefter D and A Draguhn 2017). Importantly,

genetic evidence suggests that the full extent of APP functions may be masked in APP-KO mice due to compensation by APLPs. Mice lacking only one APP family member are fully viable and show synaptic and behavioral impairments only when aged (Phinney AL et al. 1999; Ring S *et al.* 2007; Lee KJ et al. 2010). In contrast, recently generated conditional, forebrain-specific double knockout mice (termed NexCre cDKO), that lack APP in glutamatergic forebrain neurons on a global APLP2-KO background showed synaptic impairments including deficits in synaptic plasticity and cognition already as young adults (Hick M *et al.* 2015). Interestingly, early studies had shown that APP-KO mice are hypersensitive to Kainate-induced seizures (Steinbach JP et al. 1998) indicating that a lack of APP in the central nervous system (CNS) leads to diminished inhibition of the neuronal network. In addition, LTP deficits observed in aged APP-KO mice could be rescued by inhibiting $GABA_A$ receptors (Fitzjohn SM et al. 2000; Weyer SW *et al.* 2011). Thus, alterations in the GABAergic system may contribute to phenotypic abnormalities of APP/APLP2 mutant mice, but the underlying mechanisms including the specific role of APP in excitatory versus inhibitory neurons remained unknown. The importance of APP for GABAergic signaling is further highlighted by network hyperactivity both in APP overexpressing transgenic mice and AD patients (Iaccarino HF et al. 2016; Palop JJ and L Mucke 2016; Zott B et al. 2018) and the recent finding that secreted APPs can modulate the function of $GABA_BR1a$ receptors (Rice HC et al. 2019). Identifying mechanisms whereby APP impacts the GABAergic system may thus identify a link between physiological functions of APP and AD.

Here, to dissect the specific role of APP family proteins in inhibitory neurons, we generated mice lacking APP in GABAergic forebrain neurons on a global APLP2-KO background. These conditional DKO mice, termed DlxCre cDKO, exhibited a complex phenotype with impairments in hippocampus-dependent learning and memory tasks, that were associated with deficits in dendritic architecture and LTP. In addition, patch-clamp analysis of evoked responses indicated an impaired (decreased) E/I ratio that led to a reduced firing rate of

CA1 cells. Collectively, our data indicate that APP and APLP2 play a crucial role not only in excitatory neurons (Hick M *et al.* 2015) but also in GABAergic interneurons of the hippocampal network for normal synaptic plasticity, E/I balance and behavior.

Material & Methods

Mice

Experiments involving animals were performed in accordance with the guidelines and regulations set forth by the German Animal Welfare Act and the Regierungspräsidium Karlsruhe (Germany). Animals were housed in the same room with a 12 h/12 h light/dark-cycle in Makrolon Type II (360 cm^2) cages with standard bedding, either alone or in groups, and had *ad libitum* access to standard chow and water. DlxCre and $APP^{flox/flox}/APLP2^{-/-}$ mice were crossbred over several generations. Final matings were: $APP^{flox/flox}/APLP2^{-/-}$ x $APP^{flox/flox}/APLP2^{-/-}/DlxCre^{+/T}$ to obtain 50% DlxCre cDKOs (genotype: $APP^{flox/flox}/APLP2^{-/-}/DlxCre^{+}$) and 50% Cre-negative littermate (LM) controls (genotype: $APP^{flox/flox}/APLP2^{-/-}/DlxCre^{-}$). In addition, we also generated conditional single APP-KO mice, termed DlxCre cKO (genotype: $APP^{flox/flox}$/APLP2-WT/$DlxCre^{+}$) and respective Cre-negative wild type (WT) controls (genotype: $APP^{flox/flox}$/APLP2-WT/$DlxCre^{-}$). Genotyping of mice was as described previously: $APP^{flox/flox}$ (Mallm JP et al. 2010), APLP2-KO (von Koch CS et al. 1997) and DlxCre (Monory K et al. 2006). DlxCre mice were bred to Cre reporter mice (Soriano P 1999; Madisen L et al. 2010) to assess Cre expression and recombination.

AAV vector production

pAAV-mDlx-EGFP-Fishell-1 (Addgene, #83900; Dimidschstein J et al. 2016) was packaged into AAV9 capsids. Viral particles were produced as described (Richter M et al., 2018) by

transient co-transfection of HEK-293 cells with the transfer vector and the helper plasmid pDP9rs. Viral particles were purified and concentrated from cell lysate and supernatant by ultracentrifugation on an iodixanol density gradient followed by buffer exchange to 0.01% pluronic/phosphate-buffered saline (1x DPBS) via a 100 kDa Amicon centrifugal filter unit (Merck Millipore). Genome copies in the vector stocks were determined by free inverted terminal repeat (ITR)-specific quantitative TaqMan PCR and expressed as genomic copies per µl of concentrated stocks (gc/µl) as previously described (Richter M et al., 2018).

Primary hippocampal cultures and AAV transduction

For the generation of primary hippocampal cultures mouse embryos (E18-P0) were decapitated and tail samples were used for genotypization by PCR. Heads were kept in 1 ml HBSS/Glucose solution and dissected brains in 1 ml Hibernate E medium (Invitrogen) on ice for up to 4 h until completion of genotyping PCR. Hippocampi were dissected and pooled according to genotype in GBSS/Glucose solution on ice. Tissue was washed three times with 1 ml ice-cold HBSS/Glucose solution and subsequently incubated in 1 ml 1x Trypsin-EDTA (Invitrogen) for 28 min at 37°C. The trypsin solution was aspirated and the hippocampi were washed 4-5 times with wash medium (DMEM + 2% FCS). To generate a single cell suspension, 1 ml neuronal culture medium (Neurobasal medium, 2% B27, 200 mM L-Glut, 1% P/S) was added to the trypsinized tissue and the hippocampi were carefully triturated using a 2 ml syringe and cannulas with decreasing diameters (20G Ø 0.9 mm and 25G Ø 0.5 mm). The cell suspension was filtered through a cell strainer (Ø 70 µm) to remove cell debris. 150 000 cells in 500 µl neuronal culture medium per 24-well were plated on dishes with poly-L-lysine-coated coverslips. Primary hippocampal cultures were incubated at 37 °C and 5 % CO_2 until being transduced after 7 days *in vitro* (DIV7) with AAV-mDlx-EGFP-Fishell-1 (Addgene, #83900; Dimidschstein J et al. 2016) at an MOI of 4 x 10^5 in 100 µl fresh Neuronal culture medium per

24-well. On DIV14 transduced hippocampal neurons were fixed for ICC and analysis of GABAergic interneuron morphology.

Immunocytochemistry of hippocampal neurons

Neurons were washed with warm 1x DPBS once and fixed with ice-cold 4% PFA supplemented with 4% (w/v) sucrose for 5 min on ice followed by one washing step with 1x DPBS for 5 min. Fixed neurons were permeabilized with 0.1 % (v/v) Triton X-100 or 0.1% (v/v) NP40 in 1x DPBS for 10 min at room temperature and again washed with 1x DPBS for 5 min. Coverslips were blocked with 10% normal goat serum (NGS) in 1x DPBS at room temperature and for 1 h to minimize unspecific antibody binding. Primary antibodies diluted in 40 µl 1x DPBS + 5 % NGS were added onto each coverslip and incubated at room temperature for 1 h and 30 min. The following primary antibodies were used: parvalbumin (PV; guinea pig, 1:500, #195004 Synaptic Systems, Germany), calbindin (CB; rabbit, 1:500, #CB38, swant, Switzerland), calretinin (CR; rabbit, 1:500, #214102, Synaptic Systems, Germany), GFP (chicken, 1:500, #A10262, Invitrogen, USA), APP/Y188 (rabbit, 1:500, #ab32136, abcam), APLP1/CT11 (rabbit, 1:1000, Calbiochem, #not available). Coverslips were washed three times with 1x DPBS for 5-10 min and secondary antibodies diluted in 40 µl 1x DPBS + 5 % NGS were added onto each coverslip and incubated at room temperature for 30 min. The following secondary antibodies were used: anti-guinea pig Alexa 568 (1:500, #A11075, Thermo Fisher Scientific, USA), anti-rabbit Alexa 568 (1:500, #A11011, Thermo Fisher Scientific, USA), anti-rabbit Cy5 (1:500, #111-175-144, Jackson ImmunoResearch, United Kingdom), anti-chicken Alexa 488 (1:500, #A11039, Thermo Fisher Scientific, USA). After one washing step with 1x DPBS for 5 min, cells were incubated in 40 µl 1xDPBS + 0.5 µg/ml DAPI for 5 min at room temperature for nuclear staining. Finally, coverslips were briefly rinsed in MilliQ water and mounted on object slides with 10 µl Mowiol. Coverslips were dried overnight at room temperature and

sealed with nail polish on the next day. Immunostainings were analyzed with a Zeiss AxioObserver Z.1 microscope using a 20x objective (Plan-Apo 20x/0.8).

Immunostaining of brain sections

Animals were killed with CO_2 and transcardially perfused with PBS, followed by a 5 min fixation with 4% PFA in PBS. The brain was dissected from the skull and postfixed overnight at 4°C in 4% PFA in PBS. 40 µm coronal or horizontal sections were cut on a Vibratome (HM650V microtome), and collected in cold PBS in 24-well plates. Slices were blocked and permeabilized (5% BSA (w/v), 5% NGS (v/v), 0.4% Triton X-100 (w/v) in PBS) overnight at 4°C and stained free-floating in 300 µl of the appropriate dilutions of primary antibody (in PBS + 5% NGS + 0.2% Triton X-100) again overnight at 4°C. After washing with PBS, 300 µl of the corresponding secondary antibody dilutions (in PBS + 0.1% BSA + 0.05% Triton X-100) were applied and incubated for 2 h at RT. After washing the sections were stained with PBS-DAPI, collected on Superfrost microscope slides (Menzel) and mounted in Mowiol. Antibodies: parvalbumin (PV; guinea pig, 1:1,500, #195004 Synaptic Systems, Germany); calbindin (CB; rabbit, 1:3,000, #CB38, swant, Switzerland); calretinin (CR; rabbit, 1:1,500, #214102, Synaptic Systems, Germany), somatostatin (SST; rat, 1:200, #MAB354, Merck, Germany), GAD67 (mouse, 1:5,000, #MAB5406, Merck Millipore, Germany); Ctip2 (rat, 1:200, #25B6, abcam, United Kingdom); GFAP (rabbit,1:3,000, #173002, Synaptic Systems, Germany); Iba1 (rabbit, 1:500, #234003, Synaptic Systems, Germany); APP/JRD32 (mouse 1:1,000, (Hick M *et al.* 2015)); APP/Y188 (rabbit 1:500, #ab32136, abcam), goat anti-rabbit Cy3 (1:1,500, #711-165-152, Jackson ImmunoResearch Laboratories, USA); goat anti-mouse Cy5 (1:500, #A10524, Thermo Fisher Scientific, USA); goat anti-rat Alexa 488 (1:500, #112-545-167, Jackson ImmunoResearch, United Kingdom); goat anti-guinea pig Alexa 488 (1:500, #106-545-003, Jackson ImmunoResearch, United Kingdom). Images were taken with an Axio Observer Z1 (Zeiss, Germany) and a Leica TCS SP5II (Leica, Germany).

Analysis of knockout efficiency

Double immunostainings against APP (JRD32 or Y188) and the interneuron markers GAD67, PV, SST, or the medium spiny neuron (MSN) marker Ctip2 were performed using anatomically matched coronal or sagittal brain sections (40 µm) of LM control and DlxCre cDKO mice. In the hippocampal formation (HPF) the percentage of double-positive neurons ($GAD67^+/APP^+$, PV^+/APP^+, SST^+/APP^+) was analyzed in the CA1, CA3 and DG region. CB or DAPI co-staining (not depicted) was used to visualize the hippocampal subregions. While PV^+/APP^+ and SST^+/APP^+ double-positive cells were quantified in all layers of CA1, CA3 and DG, analysis of $GAD67^+/APP^+$ double-positive cells was restricted to stratum oriens (so), stratum radiatum (sr) and stratum lacunosum moleculare (slm) of CA1. Quantification of $GAD67^+$ cells was not performed in the CA3 and DG where strong immunoreactivity in neuronal processes prevented the analysis of individual cells. In the striatum (CP) the percentage of double-positive MSNs ($Ctip2^+/APP^+$) was analyzed in matched anatomical regions (coordinates:AP = 0/ML = ± 2,5/DV = ± 3,5). Images were analyzed and acquired on a Nikon C2 Plus upright confocal microscope (at the Nikon Imaging Centre at the University of Heidelberg) with a 20x objective (Plan Apo 20×/0.75). The statistical analysis was performed using GraphPad Prism version 7.04 (GraphPad, USA). Data obtained from 3 mice per genotype and 2 - 3 sequential sections per animal (n = 6 - 9 sections/genotype) were compared using an unpaired two-tailed Student's t-test. All data are indicated as mean ±SEM. Values of $p < 0.05$ were considered significant and plotted as follows *$p < 0.05$, **$p < 0.01$, ***$p < 0.001$. Data acquisition and analysis were performed blind to genotype.

Electrophysiology

In vitro extracellular recordings were performed on acute hippocampal slices of 3 - 4 month-old old DlxCre cDKOs or LM controls (n = 25 - 29 animals/genotype), DlxCre cKO or LM

controls (n = 16 - 18 animals/genotype) or 12 month-old DlxCre cKO or LM controls (n = 23 - 26 animals/genotype). In-between, animals were group-housed in a temperature- and humidity-controlled room with a 12 h light–dark cycle and had access to food and water *ad libitum*.

Slice preparation for extracellular field recordings

Acute hippocampal transversal slices were prepared from isoflurane-anesthetized individuals. Following decapitation, the brain was removed and quickly transferred into ice-cold carbogenated (95% O_2, 5% CO_2) artificial cerebrospinal fluid (ACSF) containing 125.0 mM NaCl, 2.0 mM KCl, 1.25 mM NaH_2PO_4, 2.0 mM $MgCl_2$, 26.0 mM $NaHCO_3$, 2.0 mM $CaCl_2$, and 25.0 mM glucose. The hippocampus was sectioned into 400 µm-thick transversal slices with a vibrating microtome (VT1200S, Leica, Germany) and maintained in carbogenated ACSF at room temperature for at least 1.5 h.

Extracellular field recordings

Slices were placed in a submerged recording chamber and perfused with carbogenated ACSF (32°C) at a rate of ~1.5 ml/min. Field excitatory postsynaptic potentials (fEPSPs) were recorded in stratum radiatum of CA1 region with a borosilicate glass micropipette (resistance 2–4 MΩ) filled with 3 M NaCl at a depth of ~ 150–200 µm. Monopolar tungsten electrodes were used for stimulating the Schaffer collaterals at a frequency of 0.1 Hz. Stimulation intensity was adjusted to ~ 40% of maximum fEPSP slope for 20 min baseline recording. LTP was induced by applying theta burst stimulation (TBS: 10 trains of four pulses at 100 Hz in an 200 ms interval, repeated three times).

Basal synaptic transmission properties were analyzed via input–output (IO) measurements, and short-term plasticity was examined by performing paired-pulse stimulation experiments. The IO measurements were performed either by application of defined current values (25 – 250 µA) or by adjusting the stimulus intensity to certain fiber volley (FV) amplitudes (0.1 – 0.8 mV).

Presynaptic function and short-term plasticity were assessed with the PPF paradigm by applying a pair of two closely spaced stimuli in inter-stimulus intervals (ISI) ranging from 10 to 160 ms.

Data analysis and statistics of extracellular field recordings

Data of electrophysiological recordings were collected, stored, and analyzed with LABVIEW software (National Instruments, USA). The initial slope of fEPSPs elicited by stimulation of the Schaffer collaterals was measured over time, normalized to baseline, and plotted as average ± SEM. Analysis of the PPF data was performed by calculating the ratio of the slope of the second fEPSP divided by the slope of the first one and multiplied by 100. The statistical analysis was performed using Microsoft Excel or GraphPad Prism version 6.0 (GraphPad, USA). Data obtained between two genotypes or two different experimental conditions were compared using an unpaired two-tailed Student's t-test. All data are indicated as mean ± SEM. Values of $P < 0.05$ were considered significant and plotted as follows *$P < 0.05$, **$P < 0.01$, ***$P < 0.001$. Data acquisition and analysis was performed blind to genotype.

Patch-clamp experiments

DlxCre cDKO mice and LM controls (age: 3-4 months) were used to obtain 250 µm thick acute transversal brain slices of the hippocampus. Briefly, mice were anesthetized with isoflurane and intracardially perfused with sucrose dissection (SD) solution containing 212 mM sucrose, 3 mM KCl, 1.25 mM NaH_2PO, 7 mM $MgCl_2$, 26 mM $NaHCO_3$, 0.02 mM $CaCl_2$, and 10 mM glucose. Brains were quickly removed and placed into ice-cold SD in the holding chamber of a tissue slicer (Leica, Germany; razor blade: Personna, USA). Immediately after preparation of the slices, they were incubated at 37°C for 15 min in ACSF containing 125 mM NaCl, 2.5 mM KCl, 2 mM $CaCl_2$, 1 mM $MgCl_2$, 25 mM $NaHCO_3$, 1.25 mM NaH_2PO_4, 25 mM glucose, bubbled with 95% O_2 and 5% CO_2 to pH 7.4. The holding chamber was slowly cooled down to RT and slices were incubated for 45 min before recordings. Miniature EPSCs and IPSCs were recorded using glass capillaries filled with an internal solution containing 120 mM Cs-methane

sulfonate, 8 mM NaCl, 10 mM CsCl, 0.3 mM GTP, 2 mM MgATP, 10 mM Na_2-phosphocreatine, 0.2 mM EGTA, 10 mM HEPES, pH 7.3. mEPSCs were recorded in ACSF in the presence of 10 µM SR95531 hydrobromide (gabazine; Biotrend, Germany), 50 µM APV (Biotrend, Germany) and 1 µM TTX (Biotrend, Germany) at a holding potential of -70mV. mIPSCs were recorded in ACSF in the presence of 10 µM CNQX (Biotrend, Germany), 10 µM APV (Biotrend, Germany) and 1 µM TTX at a holding potential of +10mV. Series resistance was not compensated and monitored across recordings. mEPSCs and mIPSCs were detected using a template matching algorithm in Clampfit software (Molecular Devices, USA). For recording of E/I ratios, the potential of CA1 neurons was clamped at -40mV and mixed excitatory/inhibitory currents were elicited by extracellular stimulation in the stratum radiatum in ACSF containing 50 µM APV (Biotrend, Germany). The internal solution contained 120 mM Cs-methane sulfonate, 8 mM NaCl, 10 mM CsCl, 0.3 mM GTP, 2 mM MgATP, 10 mM Na_2-phosphocreatine, 0.2 mM EGTA, 10 mM HEPES, pH 7.3. The ratio of the peaks of inward (excitatory) and outward (inhibitory) currents was calculated. For the quantification of CA1 neuron activity in response to stimulation in the stratum radiatum (i.e. activation of excitatory and inhibitory inputs), cells were first clamped at -90mV (close to the chloride reversal potential). The strength of extracellular stimulation of fibers in the stratum radiatum was adjusted to elicit excitatory postsynaptic currents with an amplitude of ~100pA. Recording mode was switched to current clamp and cells were stimulated ten times at 50Hz without changing stimulation strength. The number of elicited action potentials was counted. NMDA receptor-mediated currents were blocked with 50 µM APV (Biotrend, Germany). The internal solution contained 130mM K-Gluconate, 10mM HEPES, 10mM Phosphocreatine-Na, 10mM Na-Gluconate, 4 mM ATP-Mg-Salt, 4 mM NaCl, 0.3mM GTP, pH 7.2). Statistical analyses were performed with Graphpad Prism (Graphpad software USA). Normally distributed data were analyzed by student's t-test, not-normally distributed data were analyzed by Mann-

Whitney test. Data are presented as median ± IQR. Data acquisition and analysis was performed blind to genotype.

Neuronal morphology and spine density analysis

Biocytin fillings of hippocampal CA1 pyramidal cells

CA1 pyramidal neurons used for morphological analysis were filled with a solution containing 0.1 – 0.5 % biocytin (Sigma Aldrich, USA) through the patch-pipette while recording. Acute slices were fixed in 4 % Histofix (Carl Roth, Germany) after recording. 2 - 10 days later, the slices were washed in 1x PBS (phosphate buffered saline) for 3x 10 min. Permeabilization was performed for 1 h in 0.2 % PBST (0.2 % Triton X-100 in 1x PBS). Slices were stained overnight with Alexa 594-conjugated Streptavidin directed against biocytin (life technologies, USA). On the next day, the slices were washed again for 3x 10 min in 1x PBS. Slices were then observed under a fluorescence microscope (Olympus, Germany) to ensure that the biocytin-filled neurons were on the upper surface of the slice. After air-drying the slices at RT for 1 h they were mounted with a coverslip in ProLong Gold Antifade (life technologies, USA).

Image acquisition

Images of filled neurons were acquired on a Nikon C2 Plus or Nikon A1R upright confocal microscope (at the Nikon Imaging Centre at the University of Heidelberg). Overview images of complete neurons used for reconstruction were taken with a 20× objective (Plan Apo 20×/0.75). The complete volume of one filled neuron was imaged with a z-step size of 0.775 µm and a 1024 x 1024 (MSN) or 2048 × 2048 (CA1 pyramidal neurons) resolution. Basal and apical segments of CA1 pyramidal neurons were imaged individually with two overlapping stacks. Detailed images of dendritic segments and spines were acquired using a 40× objective (Plan Fluor 40×/1.3 oil) and a digital zoom of 4. To fulfill the Nyquist criteria for deconvolution, z-stacks of dendritic segments were captured with a pixel size of 40 nm and a z-step of 0.2 µm.

Laser power, gain and offset varied from cell to cell as the parameters were always chosen so that the complete range of the grayscale was used. Images for spine counts were deconvoluted with the Huygens Remote Manager v3.4.1 (*http://bambam.bioquant.uni-heidelberg.de/hrm/*) and saved in the TIFF format (16 bit).

Iontophoretic fillings of MSNs

In brief, striatal MSNs were visualized by postfixation filling with the negatively charged dye CF568-Hydrazide (Sigma Aldrich, Germany) in 200 µm coronal brain sections of 5.5 - 5.7-month old mice. For iontophoretic fillings of MSNs, one brain slice at a time was placed in a custom-made chamber filled with cold PBS and visualized on an Olympus BX51WI fixed stage upright microscope (Olympus, Japan). Sharp quartz glass electrodes (Quartz electrodes with filament, O.D: 1.0 mm, I.D.: 0.7 mm, 10 cm length, Sutter instruments, USA) were pulled using the Sutter P-2000 Laser Puller. The tip of the electrode was loaded with 5 mM CF568-Hydrazide dissolved in distilled water and backfilled with 0.1 M LiCl dissolved in distilled water. Using a motorized 3D micromanipulator, the electrode was lowered into the striatum (coordinates: AP = 0/ML = ± 2,5/DV = ± 3,5) under visual control using a Calcium Crimson filter cube (HQ580/20×, U-Q595LP (339038), HQ630/60 m) while applying a negative voltage pulse (-1 V, 1 Hz) to the electrode via a silver wire in line with a 500 MΩ resistor. When piercing of a cell body was observed, the cell was filled by application of a negative 1 Hz current pulse (~ 5 nA) to the electrode. Filling was for 7 min or until no further filling was observed. Afterwards, slices were fixed for 2 days in 4% PFA at 4°C, washed three times in cold PBS, and finally mounted in Mowiol.

Neuronal morphology and spine counts

Filled MSNs and CA1 pyramidal neurons were manually reconstructed using the Neurolucida software (MicroBrightField, USA) by an experimenter blind to genotype. CA1 pyramidal cells

were only included in Sholl analysis if they showed a completely filled apical or basal tree and well-defined dendritic endings. The morphometric Sholl analysis was done using the NeuroExplorer software (MicroBrightField, USA). In short, a series of concentric spheres (centered on the soma) was drawn with an intersection interval of 30 µm and the number of dendrites crossing each sphere, as well as the dendritic length in between each sphere was calculated. This analysis was done separately for basal and apical dendrites of CA1 pyramidal cells and was plotted against the distance from the soma. For evaluation of basal dendritic spine density, at least three different randomly chosen dendritic segments of the basal dendritic arbor were imaged. They had to fulfill the following criteria: (i) lie mostly horizontally to the slice surface, (ii) be at least 20 µm away from the soma, (iii) have a comparable thickness. The minimum basal dendritic length imaged per neuron was 100 µm. For evaluation of midapical dendritic spine density, at least three different dendritic segments of the apical tree were imaged. Midapical was defined as the middle third of the length of the apical dendrite measured from the origin of the apical dendrite from the soma to the endpoint of the tufts. Dendritic segments used for evaluation had to fulfill the following criteria: (i) be of second or third order to assure comparable shaft thickness, (ii) lie in the middle third of the main apical dendrite, (iii) be longer than 10 µm. The minimum midapical dendritic length imaged per neuron was 100 µm. Dendritic spines of filled MSNs or CA1 pyramidal cells were manually counted using the Neurolucida and NeuroExplorer software (MicroBrightField, USA) following the criteria of Holtmaat (Holtmaat A et al. 2009) with minor modifications: (i) All spines that protruded laterally from the dendritic shaft and exceeded a length of 0.4 µm were counted. (ii) Spines that protruded into the z-plane were only counted if they exceeded the dendritic shaft more than 0.4 µm to the lateral side. (iii) Spines that bisected were counted as two spines. (iv) Spines had to be at least 10 µm away from branching points and the soma. Spine density was expressed as spines per µm of dendrite. Prior to statistical analysis and blind to genotype, neurons were

excluded if the image quality (poor signal to noise ratio) was not sufficient for counting of spines or for deconvolution. Data acquisition and analysis was performed blind to genotype.

Analysis of interneuron morphology

EGFP expressing PV^+, CB^+, or CR^+ interneurons in pooled primary hippocampal cultures from DlxCre cDKO (Cre^+) or LM control (Cre^-) mouse embryos were imaged using a Zeiss AxioObserver Z.1 microscope and a 20x objective (Plan-Apo 20x/0.8) with an x-y and z resolution of 0.32 µm and 1 µm. For morphological analysis interneurons were manually reconstructed using the Neurolucida software (MicroBrightField, USA) and by an experimenter blind to genotype. For Sholl analysis a series of concentric spheres (centered on the soma) was drawn with an intersection interval of 30 µm and the number of dendrites crossing each sphere, as well as the dendritic length in between each sphere was calculated. Interneurons were included in morphological analysis only if they did not show any signs of degeneration such as dendrite fragmentation, retraction bulbs or a hairy soma. The statistical analysis was performed using GraphPad Prism version 7.04 (GraphPad, USA). Neuronal tracings obtained from 9 to 10 coverslips per genotype were compared using an unpaired two-tailed Student's t-test or by two-way ANOVA followed by a post hoc Sidak's multiple comparisons test (n = number of neurons/genotype). All data are indicated as mean ±SEM. Values of $p < 0.05$ were considered significant and plotted as follows *$p < 0.05$, **$p < 0.01$, ***$p < 0.001$.

Behavioral analysis

Animals

Mice (DlxCre cDKO and LM controls) were housed under a 12/12 h light–dark cycle (lights on between 8 p.m. to 8 a.m.) in groups of 2–5, unless individual housing was required by experimental protocols or to prevent fighting. Testing occurred during the dark phase under dim

light (approximately 12 lux). Mice were transferred to the testing room 30 min before testing. 16 DlxCre cDKOs (8 male, 8 female) and 16 LM controls (8 male, 8 female) were tested in the following individual tests: home cage activity (age: 1.7 – 3.6 months), nesting (age: 2.7 – 4.6 months) and burrowing (age: 2.7 – 4.6 months). The 16 females of the previous tests plus additional 5 female DlxCre cDKOs and 5 female LM controls were tested in the following IntelliCage (IC) tests: free adaptation, nose poke adaptation, drinking session adaptation, corner preference acquisition (age: 5.2 – 7.2 months), serial corner reversal (age: 5.7 – 7.6 months), corner avoidance training (age: 11.0 – 12.9 months), corner avoidance task (age: 11.0 – 12.9 months) and corner avoidance probe trial (age: 11.0 – 13.5 months). Procedures were approved by the Veterinary Office of the Kanton of Zurich (license 44/2015). Data acquisition and analysis was performed blind to genotype.

Home cage activity

Home cage activity was recorded as described previously (Madani R et al. 2003) using a cage rack equipped with one passive IR sensor per mouse (ActiviScope, New Behavior Inc., Zurich Switzerland, www.newbehavior.com). The sensors detected any locomotion and remained silent only when the mice were sleeping or grooming. Recording started after a habituation period of at least 18h and circadian activity profiles were calculated by averaging data from 11 recording days.

Nesting test

Nest building was studied as described (Deacon RM 2006). At the beginning of the dark phase, mice were placed in individual testing cages (Type II, 267 x 207 x 140 mm) in their housing room containing regular bedding and a Nestlet of 3 g compressed cotton (Ancare, Bellmore, NY). After 24h the nests were assessed on a rating scale of 1 to 5: 1 = Nestlet > 90% intact, 2

= Nestlet 50 - 90% intact, 3 = Nestlet mostly shredded but no identifiable nest site, 4 = identifiable but flat nest, 5 = crater-shaped nest.

Burrowing

Burrowing was studied as described (Deacon RM 2006). A grey plastic tube (inner diameter 6.3 cm, length 18.2 cm) was filled with 350 g standard diet food pellets (Kliba Nafag 3430, Provimi Kliba AG, Kaiseraugst, Switzerland, ca. 3 g each) and placed at a slight angle into a large standard transparent mouse cage (Type III, 425 x 266 x 155 mm). The lower end of the tube was closed, resting on the cage floor. The open end was supported 3.5 cm above the floor by two metal bolts. The cage floor was covered with fresh standard bedding material and a cardboard environmental enrichment tube was also placed in the test cage. Procedure. At the beginning of the dark period, mice were placed individually in test cages and left in their familiar animal room for an observation period of 4h after which the amount of non-displaced food was measured. This was followed by a second observation period of 20h. Water was available *ad libitum* during the entire period. It was assumed that the amount of food eaten per mouse (2 ± 0.5 g) was a very small proportion of the 350 g available and approximately equal across the groups.

IntelliCage testing

For individual identification, the mice were subcutaneously injected with RFID transponders (Datamars SA, Bedano, Switzerland). The IntelliCage (NewBehavior AG, Zurich, Switzerland) is an apparatus designed to fit inside a large cage of 20 cm high, 55 cm long and 38 cm wide at the base (Tecniplast, 2000P). The apparatus itself provides four recording chambers that fit into the corners of the housing cage covering a right-angle triangular 15 cm x 15 cm x 21 cm area of floor space each. Access into the chambers is provided via a tubular antenna (50 mm outer and 30 mm inner diameter) reading the transponder codes. The chamber, equipped with a proximity sensor, contains two openings of 13 mm diameter (one on the left, one on the right)

that give access to water bottle nipples. These openings are crossed by photo beams recording nose pokes of the mice and the holes can be closed by small motorized doors, thus barring access to water bottles in each corner. Four triangular red shelters (Tecniplast, Buguggiate, Italy) were placed in the middle of the IntelliCage and used as sleeping quarters and as a stand to reach the food. The floor was covered with a thick (2-3 cm) layer of aspen bedding (5 x 5 x 1 mm, Abedd, Lab & Vet Service GmbH, Vienna, Austria). The IntelliCage was controlled by a computer with dedicated software, executing preprogrammed experimental schedules and registering the number and duration of visits to the corners, nose pokes to the doors and lickings as behavioural measures for each mouse. Up to 13 mutant and control animals were tested together in the same cage.

Data analysis and statistics

The path of moving mice was tracked using Noldus EthoVision 3.1 (Noldus, Netherlands). For analysis, all data were imported in custom programmed software Wintrack (www.wintrack.ch; (Wolfer DP et al. 2001). Data were evaluated using a mixed ANOVA model with genotype (DlxCre cDKO and LM control) and sex as between subject factors. Within subject factors were added as needed to explore the dependence of genotype effects on place, time or stimulus. Significant interactions and where necessary significant main effects were further explored by Tukey-Kramer post-hoc tests or by splitting the ANOVA model, as appropriate. One-sample t-tests were used for follow-up comparisons against chance levels. Variables known to produce strongly skewed distributions and/or frequent outliers were subjected to a log(1+x) transformation before ANOVA analysis (as indicated, e.g. latency measures). The significance threshold was set at 0.05. The false discovery rate (FDR) control procedure of Hochberg was applied to groups of conceptually related variables within single tests to correct significance thresholds for multiple comparisons. As genotype and treatment effects were independent of sex, the sex factor is not reported in results and figures. Statistical analyses were run using R version 3.2.3 complemented with the packages psych and moments.

Results

APP is expressed in major interneuron populations and GABAergic medium spiny neurons.

Previous studies indicated high-level APP expression during development and in the adult mouse brain (Wang B et al. 2014; Hick M *et al.* 2015; Del Turco D *et al.* 2016; Schilling S *et al.* 2017), although the expression in specific neuronal subtypes has not been studied in depth. We therefore performed a detailed analysis using both WT mice (Fig. 1, S1) and NexCre cDKO mice (Fig. S1B, S2) that lack APP specifically in glutamatergic forebrain cells. Consistent with previous data, immunohistochemistry (IHC) using highly specific, validated anti-APP antibodies directed against N- or C-terminal APP epitopes (JDR32 and Y188) revealed widespread APP expression throughout the WT mouse brain (Fig. S1A). In the cortex of WT mice APP was found to be abundantly expressed in neurons of all cortical layers (Fig. 1B, C). To assess APP expression specifically in inhibitory neurons, we performed co-labeling for APP and various GABAergic markers. Consistent with APP deficiency in excitatory neurons, brain sections of NexCre cDKO mice (Fig. S1B), showed only a sparse pattern of APP^+ cells, reminiscent of interneurons. Indeed, double-immunofluorescence for GAD67, as a pan-GABAergic marker, and for APP revealed widespread APP expression in inhibitory neurons (Fig. 1, 2; Fig. S2, S5). In the hippocampus of WT mice (Fig. 1A, S1A) we detected high-level APP expression in pyramidal cells of the CA1 and CA2/3 subfields, and considerably weaker APP expression in granule cells of the dentate gyrus (DG), consistent with our previous data (Hick M *et al.* 2015; Del Turco D *et al.* 2016). Both in WT hippocampus (Fig. 1A) and in the hippocampus of NexCre cDKO mice (Fig. S1B, S2) we detected APP^+ neurons not only in principal cell layers but also in adjacent layers including the stratum oriens, the stratum radiatum, the stratum lacunosum moleculare and the hilus of the DG. To identify these cells as interneurons we stained sections of WT mice (Fig. 1A), sections of NexCre cDKO mice (Fig.

S2), or sections of Cre-negative LM controls (genotype: $APP^{flox/flox}$/APLP2-KO/Cre^{-}; see Fig. 2, S5) for APP and GAD67 (Fig. 2A), or for markers of several interneuron subtypes including parvalbumin (PV; Fig. 2B), somatostatin (SST; Fig. 2C) and calretinin (CR; Fig. S2C). Moreover, APP was also expressed in GABAergic MSNs of the striatum (Fig. S6A). Together our analysis indicates that APP is expressed not only in excitatory neurons but also in major interneuron subtypes and GABAergic striatal neurons.

Generation of mice with a conditional double knockout of APP/APLP2 in GABAergic neurons

To complement our study in NexCre cDKO mice and to assess the consequences of a lack of APP and APLP2 in inhibitory neurons we generated mice with a conditional double knockout (cDKO) of APP specifically in GABAergic forebrain neurons. To this end, we crossed $APP^{flox/flox}$APLP2-KO mice (Mallm JP *et al.* 2010) with DlxCre mice that express Cre recombinase under control of the Dlx5/6 enhancer in differentiating and migrating inhibitory neurons during embryonic development starting at around E12.5 (Taniguchi H et al., 2011; Stühmer T et al., 2002). Thus, DlxCre cDKO mice are expected to lack APP selectively in GABAergic neurons on a global APLP2 KO background. Previous studies had indicated that not every Cre line generated for gene deletion in GABAergic cells showed the anticipated widespread expression in interneuron subtypes. As a baseline for subsequent functional studies we therefore first verified the DlxCre expression pattern and recombination efficiency by crossing these mice with Ai14 and ROSA26LacZ reporter mice (see Fig. S3). We detected in both reporter lines prominent Cre expression (as indicated by tdTomato fluorescence or LacZ staining) in the main olfactory bulb (MOB), *caudate putamen* (CP) and a sparse pattern consistent with interneurons in cortex and hippocampus. Quantitative analysis of $DlxCre^{+/T}$ $Ai14^{+/T}$ mice using double immunofluorescence for GAD67 and tdTomato/Cre confirmed that the vast majority of GABAergic cells (about 96% of $GAD67^{+}$ cells in CA1 and 95% of $GAD67^{+}$

in CA3 cells, see Fig. S4) within the hippocampus co-expressed Cre recombinase. Qualitatively similar results were obtained for the cortex (data not shown). Consistently, efficient Cre recombination was also observed in major interneurons subsets studied by co-staining for PV or CR with tdTomato/Cre. In the CA1 region 94.08 ± 1.28% of the PV-expressing interneurons proved positive for Cre (Fig. S4B, C) and 92.92 ± 2.96% of the CR^+ neurons also co-expressed Cre (Fig. S4B, C). Comparable data were obtained for PV^+ and CR^+ expressing cells in the CA3 and dentate gyrus (DG), confirming that DlxCre mice are a suitable driver line for a conditional APP KO in interneurons (Fig. S4B, C).

Next, we assessed the deletion efficiency of APP in interneurons by co-staining hippocampal sections of DlxCre cDKO or LM control mice (genotype: $APP^{flox/flox}$ APLP2-KO) for GAD67/APP, PV/APP, and SST/APP, respectively (Fig. 2). Quantification indicated that APP had been very efficiently deleted in these major interneuron subsets. While in Cre-negative LM control mice about 96% of $GAD67^+$ neurons in CA1 expressed APP only 7% of $GAD67^+$ interneurons expressed APP in cDKO mice (Fig. 2A, D). APP deletion efficiency was similarly high in PV^+ and SST^+ interneurons and amounted to only 6% PV^+/APP^+ and 4% SST^+/APP^+ cells in the CA1 region of cDKO mice (Fig. 2B-D). A similar APP deletion efficiency was observed for interneurons of the CA3 region and the DG (Fig. S5A-F). Together, our analysis indicates efficient deletion of APP in major interneuron populations in DlxCre cDKO mice. In the striatum of LM control mice (Fig. 6M, O), 88% of APP expressing cells were also positive for Ctip2, identifying them as MSNs. In contrast, cDKO mice showed only 0.2% of $APP^+/Ctip2^+$double positive cells after Cre recombination in GABAergic MSNs (Fig. 6M, O). APP/APLP2 deletion did, however, not affect the number of GABAergic cells, as the number of $GAD67^+$, PV^+ or SST^+ interneurons in the adult hippocampus (Fig. S5G), as well as the number of $Ctip2^+$ MSNs in the striatum (Fig. 6N) was similar in cDKO, as compared to LM controls.

We also studied APLP1 expression to assess a potential compensatory upregulation in cDKO mice. Western blot analysis of dissected cortical and hippocampal tissue (aged 4.4 months) indicated unaltered APLP1 expression (Fig S6A-D). Previously, APLP1 expression had been demonstrated in primary mixed neuronal cultures (e.g. Schilling S et al. 2017), while expression in specific (e.g. inhibitory) neuronal subtypes had not been studied so far. To analyze APLP1 expression in interneurons, cultured neurons were first transduced with the interneuron-specific AAV vector AAV-mDlx-EGFP-Fishell-1 at DIV7 and stained with the anti-APLP1 antibody CT11 at DIV14. APLP1 expression was readily detectable in EGFP expressing interneurons (Fig S6E). Quantitative analysis of EGFP/APLP1(CT11) double-positive interneurons at DIV14 showed, however, no significant difference in APLP1(CT11) immunoreactivity in DlxCre cDKO neurons as compared to LM controls (Fig S6F).

DlxCre cDKO mice exhibit deficits in hippocampus-dependent learning and memory tasks and species-typic behavior

As our previous analysis indicated that a deletion of APP/APLP2 in excitatory forebrain neurons disturbed hippocampal function and behavior in young adult NexCre cDKO mice we first asked whether this also holds true for a deletion of APP/APLP2 in inhibitory neurons. As a baseline for subsequent cognitive tests, we first examined the neuromotor performance of DlxCre cDKO mice. Compared to LM controls, DlxCre cDKO mice showed no alteration in grip strength and normal rotarod performance (Fig. S7), indicating normal muscle strength and motor coordination, despite the lack of APP in striatal MSNs and inhibitory interneurons. Likewise, in the open field mutant mice showed no deficits in basal locomotion, explorative activity, or differences in center field avoidance indicating no obvious emotional impairments or anxiety (data not shown). In the familiar home cage we observed no difference in activity during the light phase, but DlxCre cDKO showed overshooting activity during the dark phase (Fig. 3A). Next, mice were tested in the nesting and burrowing paradigms, two species-typic

behaviors that are highly sensitive to hippocampal dysfunction (Deacon RM et al. 2002). In both tests, DlxCre cDKO mice showed major impairments (Fig. 3B, C).

To assess possible deficits in learning and memory, mice were transferred into the IntelliCage, a large home cage that permits automated testing for spontaneous behavior and various spatial learning paradigms (Fig. 3D-I; Fig. S8). Individual mice can be tracked and are tested in a social context without exposure to novelty and avoiding handling by the experimenter (see Fig. S8 for an overview of tests). In four learning corners (Fig. 3D) water can be obtained by a nose poke. After an adaptation phase during which water was freely available access to water was blocked by doors that could be opened with a nose poke, first at any time of the day, later only during 2 daily drinking sessions (11 – 12 h and 16 – 17 h, Fig. S8(1-4)). In order to study spatial learning, mice underwent a series of hippocampus-dependent test paradigms of increasing difficulty (Voikar V et al. 2010; Voikar V et al. 2018). First, each mouse was assigned a single corner in the IntelliCage where it had to obtain its water by a nose poke (corner preference task, see Fig. 3E; Fig. S8(5)). Although both groups of mice rapidly learned the task, DlxCre cDKO mice were slightly, but significantly less efficient (geno $p = 0.047$) compared to LM controls at directing their visits to the rewarded corner, particularly during the first day of training (Fig. 3E). Next, to test for behavioral flexibility and the ability for reversal learning, the mice underwent random serial reversal testing (Fig. 3F, Fig. S8(6)). In this paradigm, the availability of water was assigned in a pseudorandom fashion to a new corner at the beginning of every drinking session (twice/day), over the next 7 days. Again, both groups of mice showed learning as evidenced by an increasing percentage of correct corner visits over the training period. DlxCre mice were, however, severely impaired and showed a stable and highly significant reduction in overall performance (Fig. 3F, geno $p = 0.0096$). Together these results indicate a deficit in spatial learning and spatial memory. Subsequently, the mice were tested in an IntelliCage-adapted passive avoidance task, that depends on the functionality of the hippocampus and prefrontal cortex (Voikar V *et al.* 2010) (Fig. 3G, Fig. S8(8)). During the

training, nose pokes in one of the four learning corners were punished with an air-puff, while nose poking in the other three corners was rewarded with water. Mice underwent training for 24 h. During corner avoidance training DlxCre cDKO mutants were highly impaired and received 2.8 times (geno p = 0.011), more air puffs in the punished corner (P) as compared to LM controls (45.62 ± 10.06 in cDKOs vs 16.23 ± 3.40 in LM, see Fig 3G). Fig. 3H depicts the number of nose pokes needed to reach 10, 25, 50, 75 or 90% of the individual final performance. DlxCre cDKO mice showed a much steeper response curve to reach criterion and made considerably more errors (geno p = 0.0055). To reach 90% of their maximal performance they needed on average more than twice (2.4-fold) as many responses as LM controls (136.62 ± 21.21 in cDKO vs 57.62 ± 11.23 in LM). This avoidance deficit was not due to reduced sensitivity to air puffs, as previous testing of the mice in an IntelliCage version of the Vogel conflict test had indicated that air puffs were similarly aversive to DlxCre cDKO mutants and LM control mice (data not shown). Next, to test long term memory of the aversive situation, animals were removed from the IntelliCage and transferred for 24 h into a standard home cage, where they were deprived from water for the last 18 h of the 24 h period (Fig. S8(9)). Subsequently, the water-deprived mice were returned to their IntelliCages for the probe trial and their behavior was monitored (Fig. 3I; Fig. S8(10)). LM controls, but not DlxCre cDKO mice, showed a clear avoidance of the formerly punished corner. As such, nose poking in the formerly punished corner (P) was increased 2.2-fold in DlxCre cDKO mice (30.92 ± 3.45 in cDKOs vs 14.20 ± 2.95 in LM, geno p = 0.012). In summary, IC testing indicated deficits in spatial learning and memory, while impaired nesting and burrowing further corroborated hippocampal network dysfunction in DlxCre cDKO mice.

Behavioral impairments of DlxCre cDKO mice are associated with deficits in synaptic plasticity, disrupted E/I balance and reduced firing rate of pyramidal cells

To assess whether the deficits in hippocampus-dependent learning and memory are accompanied by alterations in hippocampus network activity, we analyzed activity-dependent synaptic plasticity in DlxCre cDKO mice (Fig. 4). After 20 min of baseline activity recording, we induced long-term potentiation (LTP) at the CA3/CA1 (Schaffer collateral) pathway by application of theta burst stimulation (TBS) in acute hippocampal slices from young adult (age: 3-4 months) DlxCre cDKO mice or APLP2-KO LM controls (genotype: $APP^{flox/flox}$/APLP2 KO). Of note, we had previously shown that mice lacking only APLP2 do not exhibit any deficits in LTP or alterations in basal synaptic transmission (Weyer SW et al. 2011; Zhang X et al. 2013). Here, DlxCre cDKO mice revealed a highly significant LTP deficit after TBS induction (see Fig. 4A) as compared to LM controls. The average potentiation analysed 55 - 60 min after TBS (t75 - 80, see Fig. 4B) in LM control slices amounted to 147 ± 4.6 % (n = 29 slices from N = 6 mice), whereas potentiation was significantly reduced in DlxCre cDKOs to 129 ± 3.8 % (n = 25 slices from N = 6 mice; unpaired Student's t-test **p < 0.001). To investigate whether the observed LTP defect is also reflected in disturbed basal synaptic properties we examined pre- and postsynaptic functionality. Comparing the fEPSP size at defined stimulus intensities revealed no significant difference between both genotypes (Fig. 4C). However, input–output strength at given fiber volley amplitudes was significantly reduced in cDKOs (Fig. 4D, unpaired Student´s t-test for 0.4 mV: *p = 0.037; for 0.5 mV: *p = 0.042). To assess whether presynaptic components are altered and thus contributing to the observed LTP deficit we investigated short-term plasticity using the paired-pulse facilitation (PPF) paradigm. Compared to LM controls DlxCre cDKO mice revealed significantly higher facilitation at shorter interstimulus intervals (ISI) of 10 ms (Fig. 4E, unpaired Student's t-test for ISI 10 ms: *p = 0.043).

Since LTP was decreased and basal excitatory synaptic transmission was altered in CA3/CA1 pyramidal cells from DlxCre cDKO mice, we investigated whether changes in synaptic currents might contribute to this effect. Synaptic physiology was studied by recording AMPA receptor-mediated mEPSCs and GABA receptor-mediated mIPSCs in CA1 pyramidal cells (Fig. 4F-K). As compared to LM controls, neither mEPSC nor mIPSC frequency or peak amplitudes were significantly changed in neurons from cDKO mice (Fig. 4F-I), indicating that the number of functional excitatory and inhibitory synapses are unaltered in cDKO mice (but see also data on morphology below). Unaltered mEPSC and mIPSC miniature amplitudes also suggest normal numbers of excitatory and inhibitory receptors at postsynaptic specializations of CA1 neurons. While action potential-independent miniature events were unchanged, the decrease in excitatory input-output strength of field potentials prompted us to analyze E/I balance of evoked responses (Fig. 4J). Of note, transgenic APP-overexpressing AD mice have previously been shown to exhibit disrupted E/I balance (Zott et al, 2018). E/I ratio was analyzed in CA1 neurons at a holding potential of -40 mV at which a compound AMPA receptor-mediated inward and $GABA_A$ receptor-mediated outward current can be recorded. Extracellular stimulation in the stratum radiatum elicits fast excitatory and slower inhibitory currents, which are delayed due to the disynaptic activation of inhibition. The ratio of peak E/I current amplitudes was reduced in cells of cDKO mice (Mann-Whitney U test, * $p = 0.0351$; see Fig. 4J). The reduction in E/I balance most likely results from decreased excitatory input strength considering the decreased input-output strength of excitatory field potentials in response to defined fiber volley amplitudes and the increased PPF indicating reduced neurotransmitter release. To investigate whether the reduction in E/I balance affects excitability of pyramidal cells, we quantified the firing frequency of pyramidal cells in response to extracellular stimulation in the stratum radiatum (i.e. activation of excitatory and inhibitory inputs; see Fig. 4K). We adjusted the stimulation strength such that the amplitude of AMPA receptor-mediated currents recorded in the voltage-clamp mode at -90 mV was approximately 100 pA and not different between genotypes,

indicating that similar numbers of excitatory fibers were activated. This stimulation elicited indeed 37% fewer action potentials in pyramidal cells of cDKO mice (unpaired Student's t-test, * p = 0.0472; see Fig. 4K). This is in line with a decreased E/I balance in DlxCre cDKO mice. Taken together with reduced input-output strength (Fig. 4D) these results indicate an imbalance of inhibitory and excitatory transmission in cDKO mice.

To investigate the contribution of individual APP family members to the LTP impairment and to assess whether a lack of APP in interneurons would be sufficient to impair synaptic plasticity we also studied DlxCre single cKO mice (genotype: $DlxCre^{+/T}/APP^{flox/flox}$/APLP2-WT). Interestingly, and in contrast to combined DlxCre cDKO mice, young adult DlxCre cKO animals of the same age (3 - 4 months old) did not show deficits in LTP (Fig. S9A, B) and revealed an overall and statistically indistinguishable increase in synaptic strength in comparison to WT controls (WT control: 139 ± 4.8 % (n = 18 slices of N = 6 mice) versus DlxCre cKO: 135 ± 4.2 % (n = 16 slices of N = 5 mice), unpaired Student´s t-test ns p = 0.568). Also, basal synaptic transmission was unaffected (Fig. S9C, D). We and others had previously observed that aging plays an important role, as global constitutive APP-KO mice are normal as young adults but develop LTP and behavioral deficits in old age (Phinney AL *et al.* 1999; Seabrook GR *et al.* 1999; Ring S *et al.* 2007). We therefore went on to analyze DlxCre cKO mice at 12-13 months of age. Indeed, aged single DlxCre cKO mice showed impaired LTP (WT control: 142 ± 6.1 % for (n = 23 slices of N = 6 mice) versus DlxCre cKO: 125 ± 3.2 % (n = 26 slices of N = 5 mice), unpaired Student´s t-test *p = 0.019; see Fig. S9E, F). Input-output strength and thus postsynaptic functionality was unaltered (Fig. S9G, H), as observed for young adult mice of the same genotype (Fig. S9(C, D). Overall, we observed LTP-deficits in young conditional APP and APLP2 double knockout mice (DlxCre cDKO), whereas single DlxCre cKO mice, lacking solely APP in interneurons, develop deficits in synaptic plasticity only when aged. Together, these findings suggest that APP and APLP2 have

overlapping functions and that APLP2 can compensate APP related deficits in DlxCre cKO mice that are unmasked in combined DlxCre cDKO mutants lacking both proteins.

Lack of APP/APLP2 in DlxCre cDKO impairs neuronal morphology of CA1 pyramidal neurons

Our previous analysis of NexCre cDKO mice lacking APP/APLP2 in excitatory neurons indicated that deficits in LTP were associated with impairments in dendritic architecture of CA1 neurons (Hick M *et al.* 2015). As interneurons are morphologically very complex and more than 20 different subtypes of interneurons have been identified in the adult hipocampus *in vivo*, we first asked whether the impairment in hippocampal network function found in DlxCre cDKO mice might also be related to a compromised morphology of hippocampal CA1 neurons. As a baseline, we first studied potential astro- or microgliosis as unspecific signs of neuroinflammation or neurodegeneration. Brain slices of DlxCre cDKO showed, however, no gross morphological abnormalities (data not shown) and showed no increase in gliosis compared to LM controls, as evidenced by unaltered GFAP or Iba1 immunoreactivity (as markers for astro- and microgliosis, respectively) in cortex, hippocampus and striatum (Fig. S10). To visualize neuronal morphology CA1 neurons (age: 4 - 5 months) were filled with biocytin through the patch-pipette and later stained with Alexa594-conjugated Streptavidin. Subsequently, biocytin filled neurons were imaged and their dendritic tree was reconstructed for Sholl analysis (Fig. 5A, B). Due to their different connectivity, the apical and basal dendrites of CA1 neurons were analyzed separately. Overall for the apical dendrite, pyramidal CA1 neurons of DlxCre cDKO mice showed no significant alteration in the total dendritic length (Fig. 5E) or total dendritic complexity (Fig. 5F). Next, we performed a more detailed analysis by plotting the dendritic length (measured within circles centered on the soma, see Fig. 5B) against the distance from the soma. In this analysis, an increased dendritic length per Sholl

sphere corresponds to an increase in dendritic complexity. Apical dendrites of cDKO CA1 neurons showed a shift in branching towards more distant dendritic segments, with a decrease in complexity in dendritic segments between 360 – 480 µm and a significant increase in complexity in more distant segments at a distance of 600 and 630 µm from the soma (Fig. 5D). In addition, we found that the maximal neurite extension (MNE) of the longest apical dendrite was significantly increased in DlxCre cDKO mice (Fig. 5C). In contrast to the rather subtle difference in branching observed for apical dendrites, basal dendrites of CA1 neurons from DlxCre cDKO mice showed a prominent reduction in total dendritic length (Fig. 5H) by about 26% (1065 ± 108.20 µm in cDKO vs 1437 ± 102.90 µm in LMs) and a highly significant reduction in the number of branching points (nodes) by 32% (6.94 ± 0.85 in cDKO vs 10.22 ± 0.84 in LMs, see Fig. 5I). This was also evident from Sholl analysis that identified a significantly reduced dendritic complexity in both proximal dendritic regions (at 30 µm and 90 µm from the soma, see Fig. 5G) and to a lesser extent also in distant regions of basal dendrites. Spine analysis revealed no significant differences in spine density between pyramidal cells of DlxCre cDKO as compared to LM control in both apical (1.66 ± 0.05 in cDKOs vs 1.74 ± 0.07 in LMs, see Fig. 5J, K) and basal dendrites (1.53 ± 0.06 in cDKOs vs 1.59 ± 0.06 in LMs, see Fig. 5J, L).

Lack of APP/APLP2 in DlxCre cDKO affects interneuron morphology

Prompted by the impaired morphology of pyramidal cells we studied interneuron morphology in primary hippocampal cultures (Fig. 6A-L). To specifically identify interneurons amongst pyramidal cells cultured neurons were transduced with AAV-mDlx-EGFP-Fishell-1 driving EGFP expression from the interneuron-specific Dlx promoter (Dimidschstein J et al. 2016). This also enabled us to trace $EGFP^+$ neurites for Sholl analysis at DIV14. Interneuron subtypes were distinguished by immunostaining against PV, CB, and CR, respectively. PV^+ interneurons

of DlxCre cDKO mice showed no significant alteration of total dendritic length (Fig 6D) or total dendritic complexity (Fig. 6C), but revealed increased complexity in specific dendritic segments at a distance of 90-120µm from the soma (Fig. 6B). CB^+ interneurons of DlxCre cDKO mice showed a highly significant increase in total dendritic length (Fig. 6H), total dendritic complexity (Fig. 6G) and increased branching at dendritic segments between 90-150 µm from the soma (Fig. 6F). No significant alterations in morphology were, however, detectable for CR^+ interneurons (Fig. 6I-L). Thus, different interneuron subtypes, are differentially affected in primary hippocampal cultures by the absence of APP/APLP2.

Lastly, we determined whether the lack of APP/APLP2 might also affect the morphology of MSNs (Fig. 6M-U), the major GABAergic principal cells of the striatum. Previous studies had indicated that a KO of widely expressed neurotrophic factors such as BDNF may differentially affect neuronal architecture of CA1 neurons and MSNs (Rauskolb S et al. 2010). MSNs were visualized in fixed tissue by iontophoretic filling with a fluorescent dye. Visual inspection of reconstructed MSNs revealed no obvious alterations (Fig. 6R) which was further confirmed by quantitative Sholl analysis (Fig. 6S). This yielded unaltered total dendritic length (Fig. 6U), unaltered dendritic complexity (Fig. 6S, T) and no significant difference in spine density (Fig. 6P, Q) in DlxCre cDKO MSNs as compared to LM controls. Together, these data indicate cell type and region-specific differences in neuronal morphology as a consequence of APP/APLP2 deficiency with deficits in dendritic complexity detected in CA1 neurons, increased complexity in specific interneuron subtypes and unaffected morphology for MSNs.

Discussion

In the hippocampus excitatory neurons account for 90% of the neuronal population whereas GABAergic interneurons represent only about 10% of all neurons (Pelkey KA et al. 2017). These interneurons encompass highly diverse cell types, which can be classified anatomically by the location of their cell bodies and neurites in different hippocampal layers, their electrophysiological properties and the expression of several marker proteins including calcium-binding proteins such as PV and neuropeptides (Pelkey KA *et al.* 2017). Despite their low number, hippocampal interneurons play a pivotal role in the control of the rhythmic output of principal cells (Allen K and H Monyer 2015) and can modulate LTP (Chen YJ et al. 2010; Huh S et al. 2016), processes that are associated with cognitive functions including memory and spatial navigation (Caroni P 2015; Ferguson BR and WJ Gao 2018). Our previous analysis of mouse mutants had indicated an important synaptic role for APP family proteins in excitatory neurons. Here, we now provide compelling evidence for a pivotal role of APP and the closely related APLP2 also in inhibitory interneurons for neuronal morphology, synaptic plasticity, E/I balance and cognition.

APP deficiency throughout the entire CNS is not associated with an obvious phenotype in young mice. In contrast, aged APP-KO mice (being 12 months or older) show reduced spine density in dendrites of hippocampal pyramidal cells, impaired LTP and hippocampus-dependent behavior (Phinney AL *et al.* 1999; Ring S *et al.* 2007; Lee KJ *et al.* 2010). No abnormalities were found in either young or old APLP2-KO mice (von Koch CS *et al.* 1997; Heber S et al. 2000; Weyer SW *et al.* 2011; Midthune B et al. 2012). Combined global constitutive APP/APLP2-DKO mice are lethal shortly after birth due to deficits in synaptic morphology and transmitter release at the neuromuscular junction (Wang P et al. 2005; Klevanski M et al. 2014). Recently generated conditional NexCre cDKO mice with a selective deletion of APP/APLP2 in excitatory forebrain neurons showed already as young adults

pronounced deficits in LTP induction and maintenance at the CA3/CA1 pathway, that was associated with a prominent reduction in spine density. Mechanistically, both transmembrane APP (Klevanski M et al. 2015) and in particular the secreted APPsα fragment are crucial for modulating synaptic strength at excitatory synapses, as demonstrated by rescue experiments with either AAV encoded APPsα, recombinant APPsα, or by genetic strategies (Hick M *et al.* 2015; Mockett BG *et al.* 2017; Richter MC *et al.* 2018; Tan VTY et al. 2018; Mockett BG et al. 2019).

Here, complementing our analysis in excitatory neurons, we selectively deleted APP in GABAergic forebrain neurons (on a global APLP2-KO background), while expression of APP in excitatory neurons was not affected. To this end, we employed the DlxCre5/6-Cre mouse line driving Cre expression in precursors of GABAergic neurons during embryonic development. Indeed, using highly sensitive Ai14 reporter mice to visualize Cre expression and IHC for interneuron markers we confirmed efficient Cre activity in various interneuron populations and GABAergic forebrain cells including medium spiny neurons of the striatum. Subsequent analysis further corroborated that the floxed APP allele underwent Cre-mediated deletion with very high efficiency (at least 90%) in DlxCre cDKO mice. Our detailed IHC analysis showed that APP is widely expressed in various interneuron subtypes. Double immunofluorescence indicated APP co-expression in the majority of $GAD67^+$ cells in all hippocampal layers and in PV and SST expressing cells, interneuron subtypes that are important for E/I balance, hippocampal rhythm generation and plasticity (Allen K and Monyer H 2015; Caroni P 2015). In addition, we detected APP expression in CR^+, CB^+ and VIP^+ interneurons (vasointestinal peptide, data not shown). These data are in line with and extend previous findings of APP expression in interneurons located in the hilus of the dentate gyrus where APP was shown to modulate adult neurogenesis within the dentate gyrus (Wang B *et al.* 2014).

Similar to hippocampus, we detected in all cortical layers interneurons (PV^+, SST^+ and VIP^+) that expressed APP but did not study co-localization in a systematic manner. Nevertheless, lack of APP/APLP2 in cortical interneurons may contribute to the behavioral abnormalities of DlxCre cDKO mice. Although APLP1 expression was not upregulated in DlxCre cDKO brain tissue or cultured interneurons we cannot formally exclude compensation at the functional level, which will await the generation of conditional triple mutants, lacking all three APP family members in interneurons.

High-level APP expression in interneurons in cortex and hippocampus suggests an important physiological function for APP in this cell type. We therefore asked whether the lack of APP in interneurons of DlxCre cDKO mice might affect the functionality of the hippocampal network. Indeed, we observed deficits in hippocampus-dependent behavior including spatial learning and memory, which were associated with deficits in LTP at the CA3/CA1 Schaffer collaterals of young adult DlxCre cDKO mice. In addition to the lack of APP, also a lack of APLP2 contributed to LTP impairments, as slices from cKO mice of similar age lacking only APP in interneurons (but that still express APLP2) showed unaltered LTP. Further analysis of basal synaptic transmission indicated impaired input-output strength in DlxCre cDKOs. The amplitude of the fiber volley is representative for the number of axons firing an action potential and serves as an estimate of the strength of an afferent input. Identical fiber volleys (e.g. 0.4 or 0.5 mV) evoked smaller fEPSP responses in DlxCre cDKO mice as compared to LM controls pointing towards impaired synaptic function. The increase in PPF suggests that presynaptic function is affected in DlxCre cDKO mice with a reduction in vesicle release probability. Unaltered frequencies and amplitudes of mEPSCs, as well as mIPSCs, exclude major alterations in the number of excitatory and inhibitory synapses of CA1 cells (but see also discussion on morphology, below), which is further supported by normal spine density. Unaltered mEPSC and mIPSC amplitudes also suggest normal numbers of AMPA and $GABA_A$ receptors at excitatory and inhibitory synapses of CA1 neurons. While action-potential independent

miniature events were unchanged, evoked responses of CA1 neurons indicated an impairment in E/I balance. This reduction in E/I ratio also resulted in a decreased excitability of pyramidal cells as evidenced by the reduced number of action potentials in response to the combined stimulation of excitatory and inhibitory inputs. In principle, reduced E/I balance may arise due to an increase in inhibition or a decrease in excitation. Taken together with the reduced input-output strength of excitatory field potentials, we favor at present a reduction in excitatory drive of CA1 neurons, which may lead to hippocampal dysfunction. Further studies are needed to assess whether restoring E/I balance (e.g. by pharmacological agents) may rescue behavioral impairments.

The unaltered density of excitatory synapses is consistent with a trans-synaptic adhesive function of APP/APLPs (Soba P et al. 2005; Schilling S *et al.* 2017) that are still expressed at the pre- and postsynaptic side of CA3/CA1 synapses. Of note, APPsα that can still be secreted by excitatory pyramidal cells may further contribute to normal synaptogenesis and/or maintenance of excitatory synapses. Despite this, we observed significant differences in the morphology of CA1 cells. In the apical dendrite of CA1 neurons branching was shifted to more distal dendritic segments (yielding a maximum between 570 - 630 µm) and the maximal extension of dendrites from the soma was significantly increased. This points to possible alterations of CA3 axonal projections and secondary sprouting of CA1 neurites searching for input. As a consequence, a subset of excitatory synapses are localized at an increased distance from the soma and will thus contribute less to the excitatory drive at the soma. Basal dendrites of CA1 cells in the stratum oriens, that receive major inputs from both CA3 and septal cholinergic neurons, were less complex and significantly shorter in DlxCre cDKOs. This, together with the shift in branching towards more distal segments of apical dendrites may further contribute to reduced E/I balance. The underlying cause of these disturbances is presently not known but may be related to overall disturbed circuitry.

Somewhat surprisingly, and in contrast to our findings in excitatory neurons of NexCre cDKO mice (Hick et al, 2015, Richter et al. 2018), we found an increase in dendritic complexity in both CB^+ and PV^+ interneurons lacking APP/APLP2. We hypothesize that this increase in complexity may reflect a compensatory sprouting-like response to diminished cell-cell and/or cell-substrate adhesion in the absence of transmembrane APP/APLP2. Whether this cell-autonomous role of APP/APLP2 in interneurons *in vitro* translates into a similar phenotype *in vivo* deserves further investigation. Of note, altered interneuron morphology may also indicate functional impairments that might contribute to decreased E/I ratio. Clearly, these important questions require a detailed morphological and electrophysiological analysis of the various interneuron subtypes in the intact hippocampus of DlxCre cDKO mice. This also includes the analysis of potential alterations in brain oscillations, that have been shown to arise due to impaired function of e. g. PV^+ basket cells (reviewed in Allen K and Monyer H 2015).

In the striatum of cDKO mice, dendritic length and branching of MSNs were unaltered, indicating that APP/APLP2 do not regulate neurite length in a cell-autonomous manner in this cell type. The striatum is very densely innervated by corticostriatal projections that contain at their terminals transmembrane APP and may thus release APPsα which may in turn mediate signals to maintain normal synaptic density. As such, we noted in striatal sections of DlxCre cDKO mice a residual APP immunoreactivity, despite cell bodies of MSNs being devoid of APP.

Impairments in hippocampal network function including reduced LTP and disturbed E/I balance were also reflected in deficits in learning and memory tasks. Using the IntelliCage we assessed acquisition learning of the spatial and temporal position of a rewarded place and further studied behavioral flexibility (Endo et al. 2011). DlxCre cDKO mice exhibited significant but rather mild impairments during corner preference learning which requires mice

to learn place discrimination of rewarded and never rewarded corners. In the more demanding random serial corner reversal test mice need to suppress their knowledge of the previously rewarded place and redirect their search for reward to a new corner that is changing in a non-predictable fashion twice per day. In this test of behavioral flexibility, DlxCre cDKO mice showed significant impairments over the whole testing period. Performance in a corner reversal test is sensitive to hippocampal lesions (Voikar V *et al.* 2018) and indicates impairments of spatial working and spatial reference memory, as mice need to remember previous visits to non-rewarded corners to optimize their strategy. Of note, behavioral flexibility has been recognized as key to executive brain functions in humans and is impaired in patients with frontal lobe damage, aging-associated cognitive decline and neuropsychological disorders (Miller EK 2000). In this regard, it is conceivable that deficits in cortical functions, which might arise due to the deletion of APP/APLP2 in cortical interneurons may contribute to the impairments of cDKO mice in this test (Rygula R et al. 2010). Cognitive deficits were also clearly evident from severely impaired performance in a spatial passive avoidance task, sensitive to hippocampal lesions (Voikar V *et al.* 2018). DlxCre cDKO mice needed substantially longer training until they learned to avoid aversive air puffs in one of the IntelliCage corners and showed impaired spatial long-term memory of the aversive experience in the probe trial. Together, this indicates hippocampal dysfunction which is further supported by impaired species-typic behaviors (nesting and burrowing) that are highly sensitive to hippocampal lesions (Deacon RM *et al.* 2002). This notion is also supported by hyperactivity and lack of habituation in the familiar home cage in the dark phase (Roberts WW et al. 1962). Lack of APP/APLP2 does however not impair all circuits involving GABAergic cells. As such, APP/APLP2 seem to be dispensable not only for the morphology of GABAergic MSNs, the major principal cells of the striatum but also for striatal function, as no major deficits in motor behaviors were detected in DlxCre cDKO mice, including unaltered locomotion in the open field, normal rotarod performance and grip strength.

Our findings show that E/I balance is compromised leading to a reduced excitability of CA1 pyramidal cells in DlxCre cDKO mice. Interestingly, hyperexcitability and neural circuit dysfunction have been associated with cognitive impairments in AD patients and AD mouse models with plaque pathology (reviewed in (Busche MA and A Konnerth 2016; Zott B *et al.* 2018)). In contrast, neuronal silencing and reduced spontaneous Ca^{2+} transients were recently reported in Tau transgenic mice (Busche MA et al. 2019; Marinkovic P et al. 2019). Moreover, the novel APP proteolytic fragment Aη also leads to neuronal silencing and impairs LTP (Willem M et al. 2015). Thus, both increased and decreased E/I balance can disrupt neuronal circuitry and affect behavior.

In summary, data from this study suggest an important physiological role for APP and APLP2 in interneurons for synaptic plasticity, neuronal network activity and cognition, functions of the nervous systems that are severely compromised in AD. Thus, a better insight into the role of APP family proteins for network homeostasis will be of high importance for developing novel treatment options.

Acknowledgment

This work was supported by grants of the Deutsche Forschungsgemeinschaft (grants within FOR1332 to U.M. and MK; grant MU-1457/14-1 and 15-1 to UM; grant CRC 1080, B11 to JvE). We are grateful to Beat Lutz for providing DlxCre mice, to Christian Buchholz (Paul Ehrlich Institut, Langen, Germany) for AAV vector production and to Julia Gobbert and Kira Gür for excellent technical assistance.

References

Allen K, Monyer H. 2015. Interneuron control of hippocampal oscillations. Curr Opin Neurobiol 31:81-87.

Busche MA, Konnerth A. 2016. Impairments of neural circuit function in Alzheimer's disease. Philos Trans R Soc Lond B Biol Sci 371.

Busche MA, Wegmann S, Dujardin S, Commins C, Schiantarelli J, Klickstein N, Kamath TV, Carlson GA, Nelken I, Hyman BT. 2019. Tau impairs neural circuits, dominating amyloid-beta effects, in Alzheimer models in vivo. Nature neuroscience 22:57-64.

Caroni P. 2015. Inhibitory microcircuit modules in hippocampal learning. Curr Opin Neurobiol 35:66-73.

Caroni P. 2015. Regulation of Parvalbumin Basket cell plasticity in rule learning. Biochem Biophys Res Commun 460:100-103.

Chen YJ, Zhang M, Yin DM, Wen L, Ting A, Wang P, Lu YS, Zhu XH, Li SJ, Wu CY, Wang XM, Lai C, Xiong WC, Mei L, Gao TM. 2010. ErbB4 in parvalbumin-positive interneurons is critical for neuregulin 1 regulation of long-term potentiation. Proc Natl Acad Sci U S A 107:21818-21823.

Dawson GR, Seabrook GR, Zheng H, Smith DW, Graham S, O'Dowd G, Bowery BJ, Boyce S, Trumbauer ME, Chen HY, Van der Ploeg LH, Sirinathsinghji DJ. 1999. Age-related cognitive deficits, impaired long-term potentiation and reduction in synaptic marker density in mice lacking the beta-amyloid precursor protein. Neuroscience 90:1-13.

Deacon RM. 2006. Assessing nest building in mice. Nat Protoc 1:1117-1119.

Deacon RM, Croucher A, Rawlins JN. 2002. Hippocampal cytotoxic lesion effects on species-typical behaviours in mice. Behav Brain Res 132:203-213.

Del Turco D, Paul MH, Schlaudraff J, Hick M, Endres K, Müller UC, Deller T. 2016. Region-Specific Differences in Amyloid Precursor Protein Expression in the Mouse Hippocampus. Front Mol Neurosci 9:134.

Dimidschstein J, Chen Q, Tremblay R, Rogers SL, Saldi GA, Guo L, Xu Q, Liu R, Lu C, Chu J, Grimley JS, Krostag AR, Kaykas A, Avery MC, Rashid MS, Baek M, Jacob AL, Smith GB, Wilson DE, Kosche G, Kruglikov I, Rusielewicz T, Kotak VC, Mowery TM, Anderson SA, Callaway EM, Dasen JS, Fitzpatrick D, Fossati V, Long MA, Noggle S, Reynolds JH, Sanes DH, Rudy B, Feng G, Fishell G. 2016. A viral strategy for targeting and manipulating interneurons across vertebrate species. Nat Neurosci 19:1743-1749.

Ferguson BR, Gao WJ. 2018. PV Interneurons: Critical Regulators of E/I Balance for Prefrontal Cortex-Dependent Behavior and Psychiatric Disorders. Front Neural Circuits 12:37.

Fitzjohn SM, Morton RA, Kuenzi F, Davies CH, Seabrook GR, Collingridge GL. 2000. Similar levels of long-term potentiation in amyloid precursor protein -null and wild-type mice in the CA1 region of picrotoxin treated slices. Neurosci Lett 288:9-12.

Heber S, Herms J, Gajic V, Hainfellner J, Aguzzi A, Rulicke T, von Kretzschmar H, von Koch C, Sisodia S, Tremml P, Lipp HP, Wolfer DP, Müller U. 2000. Mice with combined gene knock-outs reveal essential and partially redundant functions of amyloid precursor protein family members. J Neurosci 20:7951-7963.

Hefter D, Draguhn A. 2017. APP as a Protective Factor in Acute Neuronal Insults. Front Mol Neurosci 10:22.

Hick M, Herrmann U, Weyer SW, Mallm JP, Tschape JA, Borgers M, Mercken M, Roth FC, Draguhn A, Slomianka L, Wolfer DP, Korte M, Müller UC. 2015. Acute function of secreted amyloid precursor protein fragment APPsalpha in synaptic plasticity. Acta Neuropathol 129:21-37.

Holtmaat A, Bonhoeffer T, Chow DK, Chuckowree J, De Paola V, Hofer SB, Hubener M, Keck T, Knott G, Lee WC, Mostany R, Mrsic-Flogel TD, Nedivi E, Portera-Cailliau C, Svoboda K, Trachtenberg JT, Wilbrecht L. 2009. Long-term, high-resolution imaging in the mouse neocortex through a chronic cranial window. Nat Protoc 4:1128-1144.

Huh S, Baek SJ, Lee KH, Whitcomb DJ, Jo J, Choi SM, Kim DH, Park MS, Lee KH, Kim BC. 2016. The reemergence of long-term potentiation in aged Alzheimer's disease mouse model. Sci Rep 6:29152.

Iaccarino HF, Singer AC, Martorell AJ, Rudenko A, Gao F, Gillingham TZ, Mathys H, Seo J, Kritskiy O, Abdurrob F, Adaikkan C, Canter RG, Rueda R, Brown EN, Boyden ES, Tsai LH. 2016. Gamma frequency entrainment attenuates amyloid load and modifies microglia. Nature 540:230-235.

Klevanski M, Herrmann U, Weyer SW, Fol R, Cartier N, Wolfer DP, Caldwell JH, Korte M, Müller UC. 2015. The APP Intracellular Domain Is Required for Normal Synaptic Morphology, Synaptic Plasticity, and Hippocampus-Dependent Behavior. J Neurosci 35:16018-16033.

Klevanski M, Saar M, Baumkotter F, Weyer SW, Kins S, Müller UC. 2014. Differential role of APP and APLPs for neuromuscular synaptic morphology and function. Mol Cell Neurosci 61C:201-210.

Kohli BM, Pflieger D, Mueller LN, Carbonetti G, Aebersold R, Nitsch RM, Konietzko U. 2012. Interactome of the amyloid precursor protein APP in brain reveals a protein network involved in synaptic vesicle turnover and a close association with Synaptotagmin-1. J Proteome Res 11:4075-4090.

Lassek M, Weingarten J, Einsfelder U, Brendel P, Müller U, Volknandt W. 2013. Amyloid precursor proteins are constituents of the presynaptic active zone. J Neurochem 127:48-56.

Lazarevic V, Fienko S, Andres-Alonso M, Anni D, Ivanova D, Montenegro-Venegas C, Gundelfinger ED, Cousin MA, Fejtova A. 2017. Physiological Concentrations of Amyloid Beta Regulate Recycling of Synaptic Vesicles via Alpha7 Acetylcholine Receptor and CDK5/Calcineurin Signaling. Front Mol Neurosci 10:221.

Lee KJ, Moussa CE, Lee Y, Sung Y, Howell BW, Turner RS, Pak DT, Hoe HS. 2010. Beta amyloid-independent role of amyloid precursor protein in generation and maintenance of dendritic spines. Neuroscience 169:344-356.

Ludewig S, Korte M. 2016. Novel Insights into the Physiological Function of the APP (Gene) Family and Its Proteolytic Fragments in Synaptic Plasticity. Front Mol Neurosci 9:161.

Madani R, Kozlov S, Akhmedov A, Cinelli P, Kinter J, Lipp HP, Sonderegger P, Wolfer DP. 2003. Impaired explorative behavior and neophobia in genetically modified mice lacking or overexpressing the extracellular serine protease inhibitor neuroserpin. Mol Cell Neurosci 23:473-494.

Madisen L, Zwingman TA, Sunkin SM, Oh SW, Zariwala HA, Gu H, Ng LL, Palmiter RD, Hawrylycz MJ, Jones AR, Lein ES, Zeng H. 2010. A robust and high-throughput Cre reporting and characterization system for the whole mouse brain. Nature neuroscience 13:133-140.

Mallm JP, Tschape JA, Hick M, Filippov MA, Müller UC. 2010. Generation of conditional null alleles for APP and APLP2. Genesis 48:200-206.

Marinkovic P, Blumenstock S, Goltstein PM, Korzhova V, Peters F, Knebl A, Herms J. 2019. In vivo imaging reveals reduced activity of neuronal circuits in a mouse tauopathy model. Brain 142:1051-1062.

Midthune B, Tyan SH, Walsh JJ, Sarsoza F, Eggert S, Hof PR, Dickstein DL, Koo EH. 2012. Deletion of the amyloid precursor-like protein 2 (APLP2) does not affect hippocampal neuron morphology or function. Mol Cell Neurosci 49:448-455.

Miller EK. 2000. The prefrontal cortex and cognitive control. Nat Rev Neurosci 1:59-65.

Mockett BG, Guevremont D, Elder MK, Parfitt KD, Peppercorn K, Morrissey J, Singh A, Hintz TJ, Kochen L, Tom Dieck S, Schuman E, Tate WP, Williams JM, Abraham WC. 2019. Glutamate Receptor Trafficking and Protein Synthesis Mediate the Facilitation of LTP by Secreted Amyloid Precursor Protein-Alpha. J Neurosci 39:3188-3203.

Mockett BG, Richter M, Abraham WC, Müller UC. 2017. Therapeutic Potential of Secreted Amyloid Precursor Protein APPsalpha. Front Mol Neurosci 10:30.

Monory K, Massa F, Egertova M, Eder M, Blaudzun H, Westenbroek R, Kelsch W, Jacob W, Marsch R, Ekker M, Long J, Rubenstein JL, Goebbels S, Nave KA, During M, Klugmann M, Wolfel B, Dodt HU, Zieglgansberger W, Wotjak CT, Mackie K, Elphick MR, Marsicano G, Lutz B. 2006. The endocannabinoid system controls key epileptogenic circuits in the hippocampus. Neuron 51:455-466.

Müller UC, Deller T, Korte M. 2017. Not just amyloid: physiological functions of the amyloid precursor protein family. Nat Rev Neurosci 18:281-298.

Palop JJ, Mucke L. 2016. Network abnormalities and interneuron dysfunction in Alzheimer disease. Nature Reviews Neuroscience 17:777.

Pelkey KA, Chittajallu R, Craig MT, Tricoire L, Wester JC, McBain CJ. 2017. Hippocampal GABAergic Inhibitory Interneurons. Physiol Rev 97:1619-1747.

Phinney AL, Calhoun ME, Wolfer DP, Lipp HP, Zheng H, Jucker M. 1999. No hippocampal neuron or synaptic bouton loss in learning-impaired aged beta-amyloid precursor protein-null mice. Neuroscience 90:1207-1216.

Rauskolb S, Zagrebelsky M, Dreznjak A, Deogracias R, Matsumoto T, Wiese S, Erne B, Sendtner M, Schaeren-Wiemers N, Korte M, Barde YA. 2010. Global deprivation of brain-derived neurotrophic factor in the CNS reveals an area-specific requirement for dendritic growth. J Neurosci 30:1739-1749.

Rice HC, de Malmazet D, Schreurs A, Frere S, Van Molle I, Volkov AN, Creemers E, Vertkin I, Nys J, Ranaivoson FM, Comoletti D, Savas JN, Remaut H, Balschun D, Wierda KD, Slutsky I, Farrow K, De Strooper B, de Wit J. 2019. Secreted amyloid-beta precursor protein functions as a GABABR1a ligand to modulate synaptic transmission. Science 363.

Richter MC, Ludewig S, Winschel A, Abel T, Bold C, Salzburger LR, Klein S, Han K, Weyer SW, Fritz AK, Laube B, Wolfer DP, Buchholz CJ, Korte M, Müller UC. 2018. Distinct in vivo roles of secreted APP ectodomain variants APPsalpha and APPsbeta in regulation of spine density, synaptic plasticity, and cognition. EMBO J 37.

Ring S, Weyer SW, Kilian SB, Waldron E, Pietrzik CU, Filippov MA, Herms J, Buchholz C, Eckman CB, Korte M, Wolfer DP, Müller UC. 2007. The secreted beta-amyloid precursor protein ectodomain APPs alpha is sufficient to rescue the anatomical, behavioral, and electrophysiological abnormalities of APP-deficient mice. J Neurosci 27:7817-7826.

Roberts WW, Dember WN, Brodwick M. 1962. Alternation and exploration in rats with hippocampal lesions. J Comp Physiol Psychol 55:695-700.

Rygula R, Walker SC, Clarke HF, Robbins TW, Roberts AC. 2010. Differential contributions of the primate ventrolateral prefrontal and orbitofrontal cortex to serial reversal learning. J Neurosci 30:14552-14559.

Schilling S, Mehr A, Ludewig S, Stephan J, Zimmermann M, August A, Strecker P, Korte M, Koo EH, Müller UC, Kins S, Eggert S. 2017. APLP1 Is a Synaptic Cell Adhesion Molecule, Supporting Maintenance of Dendritic Spines and Basal Synaptic Transmission. J Neurosci 37:5345-5365.

Seabrook GR, Smith DW, Bowery BJ, Easter A, Reynolds T, Fitzjohn SM, Morton RA, Zheng H, Dawson GR, Sirinathsinghji DJ, Davies CH, Collingridge GL, Hill RG. 1999. Mechanisms contributing to the deficits in hippocampal synaptic plasticity in mice lacking amyloid precursor protein. Neuropharmacology 38:349-359.

Selkoe DJ. 2002. Alzheimer's disease is a synaptic failure. Science 298:789-791.

Soba P, Eggert S, Wagner K, Zentgraf H, Siehl K, Kreger S, Lower A, Langer A, Merdes G, Paro R, Masters CL, Müller U, Kins S, Beyreuther K. 2005. Homo- and heterodimerization of APP family members promotes intercellular adhesion. Embo J 24:3624-3634.

Soriano P. 1999. Generalized lacZ expression with the ROSA26 Cre reporter strain. Nat Genet 21:70-71.

Steinbach JP, Müller U, Leist M, Li ZW, Nicotera P, Aguzzi A. 1998. Hypersensitivity to seizures in beta-amyloid precursor protein deficient mice. Cell Death Differ 5:858-866.

Stühmer T, Puelles L, Ekker M, Rubenstein JL. 2002. Expression from a Dlx gene enhancer marks adult mouse cortical GABAergic neurons. Cereb Cortex 12:75-85.

Tan VTY, Mockett BG, Ohline SM, Parfitt KD, Wicky HE, Peppercorn K, Schoderboeck L, Yahaya MFB, Tate WP, Hughes SM, Abraham WC. 2018. Lentivirus-mediated expression of human secreted amyloid precursor protein-alpha prevents development of memory and plasticity deficits in a mouse model of Alzheimer's disease. Mol Brain 11:7.

Taniguchi H, He M, Wu P, Kim S, Paik R, Sugino K, Kvitsiani D, Fu Y, Lu J, Lin Y, Miyoshi G, Shima Y, Fishell G, Nelson SB, Huang ZJ. 2011. A resource of Cre driver lines for genetic targeting of GABAergic neurons in cerebral cortex. Neuron 71:995-1013.

Terry RD, Masliah E, Salmon DP, Butters N, DeTeresa R, Hill R, Hansen LA, Katzman R. 1991. Physical basis of cognitive alterations in Alzheimer's disease: synapse loss is the major correlate of cognitive impairment. Annals of neurology 30:572-580.

Tyan SH, Shih AY, Walsh JJ, Maruyama H, Sarsoza F, Ku L, Eggert S, Hof PR, Koo EH, Dickstein DL. 2012. Amyloid precursor protein (APP) regulates synaptic structure and function. Mol Cell Neurosci 51:43-52.

Voikar V, Colacicco G, Gruber O, Vannoni E, Lipp HP, Wolfer DP. 2010. Conditioned response suppression in the IntelliCage: assessment of mouse strain differences and effects of hippocampal and striatal lesions on acquisition and retention of memory. Behav Brain Res 213:304-312.

Voikar V, Krackow S, Lipp HP, Rau A, Colacicco G, Wolfer DP. 2018. Automated dissection of permanent effects of hippocampal or prefrontal lesions on performance at spatial, working memory and circadian timing tasks of C57BL/6 mice in IntelliCage. Behav Brain Res 352:8-22.

von Koch CS, Zheng H, Chen H, Trumbauer M, Thinakaran G, van der Ploeg LH, Price DL, Sisodia SS. 1997. Generation of APLP2 KO mice and early postnatal lethality in APLP2/APP double KO mice. Neurobiol Aging 18:661-669.

Wang B, Wang Z, Sun L, Yang L, Li H, Cole AL, Rodriguez-Rivera J, Lu HC, Zheng H. 2014. The amyloid precursor protein controls adult hippocampal neurogenesis through GABAergic interneurons. J Neurosci 34:13314-13325.

Wang P, Yang G, Mosier DR, Chang P, Zaidi T, Gong YD, Zhao NM, Dominguez B, Lee KF, Gan WB, Zheng H. 2005. Defective neuromuscular synapses in mice lacking amyloid precursor protein (APP) and APP-Like protein 2. J Neurosci 25:1219-1225.

Weyer SW, Klevanski M, Delekate A, Voikar V, Aydin D, Hick M, Filippov M, Drost N, Schaller KL, Saar M, Vogt MA, Gass P, Samanta A, Jaschke A, Korte M, Wolfer DP,

Caldwell JH, Müller UC. 2011. APP and APLP2 are essential at PNS and CNS synapses for transmission, spatial learning and LTP. EMBO J 30:2266-2280.

Weyer SW, Zagrebelsky M, Herrmann U, Hick M, Ganss L, Gobbert J, Gruber M, Altmann C, Korte M, Deller T, Müller UC. 2014. Comparative analysis of single and combined APP/APLP knockouts reveals reduced spine density in APP-KO mice that is prevented by APPsalpha expression. Acta neuropathologica communications 2:36.

Wilhelm BG, Mandad S, Truckenbrodt S, Krohnert K, Schafer C, Rammner B, Koo SJ, Classen GA, Krauss M, Haucke V, Urlaub H, Rizzoli SO. 2014. Composition of isolated synaptic boutons reveals the amounts of vesicle trafficking proteins. Science 344:1023-1028.

Willem M, Tahirovic S, Busche MA, Ovsepian SV, Chafai M, Kootar S, Hornburg D, Evans LD, Moore S, Daria A, Hampel H, Muller V, Giudici C, Nuscher B, Wenninger-Weinzierl A, Kremmer E, Heneka MT, Thal DR, Giedraitis V, Lannfelt L, Müller U, Livesey FJ, Meissner F, Herms J, Konnerth A, Marie H, Haass C. 2015. eta-Secretase processing of APP inhibits neuronal activity in the hippocampus. Nature 526:443-447.

Wolfer DP, Madani R, Valenti P, Lipp HP. 2001. Extended analysis of path data from mutant mice using the public domain software Wintrack. Physiol Behav 73:745-753.

Yang G, Gong YD, Gong K, Jiang WL, Kwon E, Wang P, Zheng H, Zhang XF, Gan WB, Zhao NM. 2005. Reduced synaptic vesicle density and active zone size in mice lacking amyloid precursor protein (APP) and APP-like protein 2. Neurosci Lett 384:66-71.

Zhang X, Herrmann U, Weyer SW, Both M, Müller UC, Korte M, Draguhn A. 2013. Hippocampal network oscillations in APP/APLP2-deficient mice. PLoS One 8:e61198.

Zott B, Busche MA, Sperling RA, Konnerth A. 2018. What Happens with the Circuit in Alzheimer's Disease in Mice and Humans? Annu Rev Neurosci 41:277-297.

Zou C, Crux S, Marinesco S, Montagna E, Sgobio C, Shi Y, Shi S, Zhu K, Dorostkar MM, Müller UC, Herms J. 2016. Amyloid precursor protein maintains constitutive and adaptive plasticity of dendritic spines in adult brain by regulating D-serine homeostasis. EMBO J 35.

Caption of figures

Figure 1: APP is expressed in GABAergic interneurons within the hippocampus and cortex. Double-immunohistochemistry (IHC) of coronal brain sections (40 µm) of wild type (WT) mice (age: 4.4 month) stained with the APP-specific antibody Y188 (red) and the interneuron marker GAD67 (green). (**A**) APP immunoreactivity is detected in pyramidal CA1 neurons and to a much lesser extent in granule cells of the dentate gyrus. Note that neurons in layers adjacent to principal cells express APP. These APP$^+$ neurons are interneurons, identified by GAD67 expression. Within the hilus of the DG both APP and GAD67 staining is not confined to cell bodies but also prominent in neurites. Exemplary APP$^+$/GAD67$^+$ cells are indicated by arrowheads. The intensity of APP staining in somata of CA1 cells was overexposed to visualize expression in interneurons. (**B**) somatosensory cortex (CTX). APP$^+$/GAD67$^+$ IHC identifies APP expression in interneurons. (**C**) higher magnification of boxed area. The asterisk marks green autofluorescent debris. Representative confocal images taken from 2 WT animals. Scale bars hippocampus (HC), CTX: 200 µm.

Figure 2: APP is efficiently deleted in interneurons of DlxCre cDKO mice. (A, B, C) Hippocampal sections (40 µm) of DlxCre cDKOs and littermate (LM) control mice were stained for the following interneuron markers (green): GAD67 (**A**), parvalbumin (PV, **B**) or somatostatin (SST; **C**) and in addition for APP (JRD32, red) to assess the APP knockout efficiency in the CA1 region. Arrowheads indicate double positive cells in LMs, while APP staining was absent in cDKO interneurons. Representative confocal images from 3 mice/genotype. **(D)** Graphs indicate the percentage of interneurons (GAD$^+$, Parv$^+$, SST$^+$) that express APP in LM controls versus cDKO mice. Note the efficient deletion of APP in interneurons of cDKO mice. Unpaired Student's t-test, n = 6 - 9 sections from 3 mice/genotype, ****p<0.0001. Error bars indicate mean ± SEM. Scale bars (A, B, C): 200 µm.

Figure 3: DlxCre cDKOs show deficits in species-typic tasks and impairments in learning and memory (A) Home cage activity: Home cage activity during the dark and light phase after 24h of habituation. Dark phase activity was strongly increased in DlxCre cDKO (red circle) compared to littermate (LM) control (grey circle) mice (geno $F(1,26) = 11.2$ $p = 0.0025$; phase $F(1,26) = 339.6$ $p < 0.0001$; phase x geno $F(1,26) = 19.5$ $p = 0.0002$). n = 15 animals/genotype. Sex: 7 males, 8 females per genotype. **(B) Burrowing**: Pellets removed from tube after 4h and 24h. Maximum to be removed = 350g. Burrowing behavior was impaired in DlxCre cDKOs (geno $F(1,28) = 4.3$ $p = 0.0464$; time $F(1,28) = 51.0$ $p < 0.0001$; time x geno $F(1,28) = 1.7$ ns). n=16 animals/genotype. Sex: 8 males, 8 females per genotype. **(C) Nesting**: Nesting score 24h after nesting material was provided, scale: scores of 1-5. Nest quality of DlxCre cDKOs was poorer than in LM controls (geno $F(1,28) = 6.9$ $p = 0.0141$). n = 16 animals/genotype. Sex: 8 males, 8 females per genotype**. (D) Intellicage (IC)** - Overview. **(E) IC, Corner preference learning**: Correct visits with nose pokes (%) as a function of the training day (day 0 = baseline with all corners correct). DlxCre cDKOs were impaired at the beginning of training (geno $F(1,24) = 4.4$ $p = 0.0471$; time $F(3,72) = 516.9$ $p < 0.0001$; time x geno $F(3,72) = 2.8$ $p = 0.0440$). n = 13 animals/genotype. Sex: all females. **(F) IC, Serial corner reversal**: Correct visits with nose pokes (%) as a function of the training day (day 0 = last day of corner preference reversal). cDKOs were strongly impaired throughout training (geno $F(1,24)=7.9$ $p=0.0096$; time $F(3,72) = 37.8$ $p < 0.0001$; time x geno $F(3,72) = 3.3$ $p = 0.0244$). n = 13 animals/genotype. **(G) IC, Corner avoidance training**: Number of air puffs delivered to left (L), punished (P), right (R) and opposite (O) corners during the training day. DlxCre cDKOs received more air puffs in the punished corner (geno $F(1,24) = 7.7$ $p = 0.0107$; corner $F(3,72) = 33.9$ $p < 0.0001$; corner x geno $F(3,72) = 7.7$ $p = 0.0002$). n = 13 animals/genotype. **(H) IC, Corner avoidance task**: Number of responses needed to reach 10%, 25%, 50%, 75%, 90% of individual final performance. DlxCre cDKO mice made significantly more errors until they reached final

performance (geno F(1,24) = 9.3 p = 0.0055; level F(4,96) = 35.2 p < 0.0001; level x geno F(4,96) = 7.1 p < 0.0001). n=13 animals/genotype. **(I) IC, Corner avoidance probe trial**: Nose pokes (%) in formerly punished (P), left (L), opposite (O) and right (R) corner during the corner avoidance probe trial. LM controls but not DlxCre cDKOs showed clear avoidance of the formerly punished corner. DlxCre cDKO mice made more pokes in the formerly punished corner than controls (geno F(1,24) = 0.649 p = 0.4285; corner F(3,72) = 0.365 p = 0.7781; geno x corner F(3,72) = 3.905 p = 0.0121). n = 13 animals/genotype. Date are represented as mean ± SEM. Data were analyzed using mixed ANOVA models with genotype (DlxCre cDKO vs. LM control) as between subject factor and within subject factors to explore the dependence of genotype effects on place, time, or stimulus. Significant interactions and where necessary significant main effects were further explored by Tukey-Kramer post-hoc tests or by splitting the ANOVA model, as appropriate. One-sample t-tests were used for follow-up comparisons against chance levels. The significance threshold was set at 0.05. The false discovery rate (FDR) control procedure of Hochberg was applied to groups of conceptually related variables within single tests to correct significance thresholds for multiple comparisons. *p < 0.05, **p < 0.01, ***p < 0.001.

Figure 4: DlxCre cDKO mice reveal impairments of the hippocampal network including deficits in LTP and disturbed E/I balance. (A, B) LTP was induced by theta burst stimulation (TBS; black arrowhead) in acute slices after 20 min of baseline activity recording. TBS led to an overall increase of synaptic efficacy in littermate (LM) controls (147 ± 4.6 %, grey circles) which was significantly reduced in DlxCre cDKO (129 ± 3.8 %, red circles) 60 min after TBS (t75-80; unpaired Student´s t-test, ** p = 0.005). Insets show original traces of representative individual experiments. Vertical scale bar = 1 mV, horizontal scale bar = 5 ms. **(C, D)** While a correlation of given stimulus intensities to fEPSP slope showed no overt deficit, the correlation

to defined fiber volley amplitudes pointed towards reduced input-output strength in DlxCre cDKOs (unpaired Student´s t-test, 0.4 mV: * p = 0.037, 0.5 mV: * p = 0.042). **(E)** Paired-pulse stimulation revealed a significant defect of short-term plasticity at ISI 10 ms (unpaired Student´s t-test, * p = 0.043) n = number of slices. N = number of animals (age: 3 – 4 months). Data are represented as mean ± SEM. **(F–G)** mEPSC peak amplitude in CA1 pyramidal cells reveals no difference between genotypes while mEPSC event frequency shows a trend towards reduction, although not significant (ns). **(F)** mEPSC sample traces of recordings from CA1 pyramidal cells in the presence of TTX, APV, and gabazine (red: cDKO; black: LM control). **(G)** mEPSC peak amplitude and frequency in CA1 pyramidal cells is similar between genotypes. Left: Bar graph of the median peak amplitudes of mEPSCs. Right: Bar graph of the median mEPSC frequency. Data are represented as median ± IQR. **(H)** mIPSC sample traces of recordings from CA1 pyramidal cells in the presence of TTX, APV, and CNQX (red: cDKO; black: LM control) and control recordings in the presence of gabazine. **(I)** mIPSC peak amplitude and frequency in CA1 pyramidal cells is similar between genotypes. Left: Bar graph of the median peak amplitudes of mIPSCs. Right: Bar graph of the median mIPSC frequency. n = number of neurons from 4 animals/genotype (age: 4 months). Data are represented as median ± IQR. (**J**) E/I ratio is decreased in CA1 pyramidal cells of DlxCre cDKOs. Left: sample traces from mixed excitatory/inhibitory currents recorded at a holding potential of -40mV. Right: Bar graph of the median E/I ratios (± IQRs). Mann-Whitney U test, *p< 0.05 . n = number of neurons from 4 LM and 3 DlxCre cDKO mice (age: 4 months). (**K**) CA1 pyramidal cells of DlxCre cDKOs are hypoexcitable compared to cells of LMs. Left: sample action potential traces elicited with ten stimulations of CA3 inputs (50Hz). (Right) Bar graphs of the peak amplitude of AMPA receptor-mediated currents recorded in voltage clamp at -70mV and the number of action potentials recorded in current clamp (mean ± SEM). Unpaired Student´s t-test, * p < 0.05, n = number of neurons from 4 LM and 3 DlxCre cDKO mice (age: 4 months).

Figure 5: Lack of APP/APLP2 in GABAergic interneurons leads to reduced neurite length and impaired branching of CA1 pyramidal neurons.

(A) Representative 3D-reconstructions of CA1 pyramidal neurons from littermate (LM) control (left) and DlxCre cDKO (cDKO) mice (right). **(B)** Schematic representation of parameters assessed. **(C)** DlxCre cDKO neurons show a significantly increased maximal neurite extension (MNE) of apical dendrites compared to LM controls (Unpaired Student´s t-test, ** p = 0.0022). **(D)** Sholl analysis reveals a significant genotype effect on apical dendritic morphology (two-way repeated measures ANOVA: genotype F(1, 34) = 0,1315, p = 0.7192, with post hoc Sidak's multiple comparisons test * p < 0.05, ***p < 0.001). **(E, F)** Compared to LM controls, CA1 neurons of DlxCre cDKOs show no significant reduction in total dendritic length or branching in apical dendrites. **(G)** Scholl analysis reveals a significant overall genotype effect on basal dendritic morphology (two-way repeated measures ANOVA: genotype F(1, 34) = 6,637, p = 0.0145, with post hoc Sidak's multiple comparisons test ** p < 0.01, **** p < 0.0001). **(H, I)** Compared to LM controls, DlxCre cDKO neurons show a significantly reduced total dendritic length and impaired branching of basal dendrites (Unpaired Student´s t-test, * p = 0.0177, ** p = 0.0099). n = number of neurons from 6 animals/genotype (age: 3.5 month). **(J)** Representative confocal images of dendrites from LM control (top) and DlxCre cDKO mice (bottom). Images are maximum projections of deconvoluted z-stacks. n = number of neurons from 6 animals/genotype (age: 3.5 month). **(K, L)** Spine densities of basal dendrites or apical dendrites of Biocytin-filled hippocampal CA1 neurons do not differ significantly between genotypes (unpaired Student's t-test, n =18 neurons, p = 0.8999 or 0.3278, ns = not significant). For spine density analysis at least 100 µm of dendritic length/neuron were analyzed. Data are represented as mean ± SEM.

Figure 6: Lack of APP/APLP2 in GABAergic interneurons affects neuronal morphology of hippocampal interneurons, while medium spiny neuron morphology is normal

(A-L) Morphological analysis of interneuron subtypes in primary hippocampal cultures at DIV14. Representative 3D-reconstructions of PV^+ **(A)**, CB^+ **(E)** and CR^+ **(I)** interneurons from LM control (left; black) and DlxCre cDKO mice (right; red). **(B)** Sholl analysis of PV^+ interneurons reveals a significant genotype effect on dendritic morphology (Two-way repeated measures ANOVA: genotype $F(1,36) = 0.5473$, $p = 0.4642$, post hoc Sidak's multiple comparisons tests, $*p < 0.05$). The total number of dendritic intersections (**C**) and total dendritic length (**D**) are not significantly different between genotypes (Unpaired student's t-test, two-tailed, n (neurons) = 19, p = 0.4642 or 0.8459, ns). **(F)** Sholl analysis of CB^+ interneurons shows a significant genotype effect on dendritic morphology (Two-way repeated measures ANOVA: genotype $F(1,37) = 19.21$, $p<0.0001$, with post hoc Sidak's multiple comparisons tests, $**p<0.01$, $****p<0.0001$). The total number of dendritic intersections (G) and total dendritic length (**H**) are significantly different between genotypes (Unpaired student's t-test, two-tailed, n (neurons) = 19 or 20, $***p<0.0001$). **(J)** Sholl analysis of CR^+ interneurons indiactes no significant genotype effect on dendritic morphology (Two-way repeated measures ANOVA: genotype $F(1,28) = 2.929$, $p = 0.0981$, with post hoc Sidak's multiple comparisons tests, ns = not significant). The total number of dendritic intersections (**K**) and the total dendritic length (**L**) are not significantly different between genotypes (Unpaired student's t-test, two-tailed, n (neurons) = 14 or 16, p = 0.0981 or 0.1426, ns = not significant). Error bars indicate ± SEM.

(M) Anatomically matched sagittal brain sections (40 µm) of LM controls and DlxCre cDKO mice were stained using the APP-specific antibody JRD32 (red), and the medium spiny neuron (MSN) marker Ctip2 (green). Note the somatic APP localization in compartments of the secretory pathway while Ctip2 is found in the nucleus. Representative images of n = 3 animals/genotype (age: 1-month-old). **(N)** The number of $Ctip2^+$ cells in the striatum (CP,

caudate putamen) is similar between genotypes. **(O)** Compared to LM controls only 0.2% of Ctip2$^+$ MSNs in the CP of cDKOs are positive for APP, indicating efficient APP deletion in MSNs in DlxCre cDKO mice. Analyzed cell bodies are highlighted by a small white cross. Unpaired student's t-test, two-tailed, n (sections) = 9, **** $p < 0.0001$, ns = not significant)**.**

(R-U) Sholl analysis and spine density counts were performed upon iontophoretic postfixation fillings, **(P)** Representative confocal images of MSN dendrites from LM control (left) and DlxCre cDKO mice (right). Images are maximum projections of deconvoluted z-stacks. **(Q)** Spine densities of secondary and tertiary dendrites of MSNs do not differ significantly between genotypes (Unpaired student's t-test, two-tailed, n (neurons) = 40 or 36, $p = 0.0673$, ns = not significant). For spine density analysis at least 150 µm and up to 200 µm of each neuron were analyzed. **(R)** Representative 3D-reconstructions of MSNs from LM control (left) and DlxCre cDKO mice (right). **(S)** Sholl analysis reveals no significant overall genotype effect on dendritic morphology (Two-way repeated measures ANOVA: genotype $F(1,77) = 0.1556$, $p = 0.6943$, with post hoc Sidak's multiple comparisons tests, ns = not significant). The total number of dendritic intersections (**T**) and the total dendritic length (**U**) are not significantly different between genotypes (Unpaired student's t-test, two-tailed, n (neurons) = 40, $p = 0.5968$ or 0.3903, ns = not significant). **(M -U)** n = number of neurons (4 animals/genotype, age: 5.5 – 5.7-month-old). Error bars indicate ± SEM. Scale bars (D, G): 20 µm.

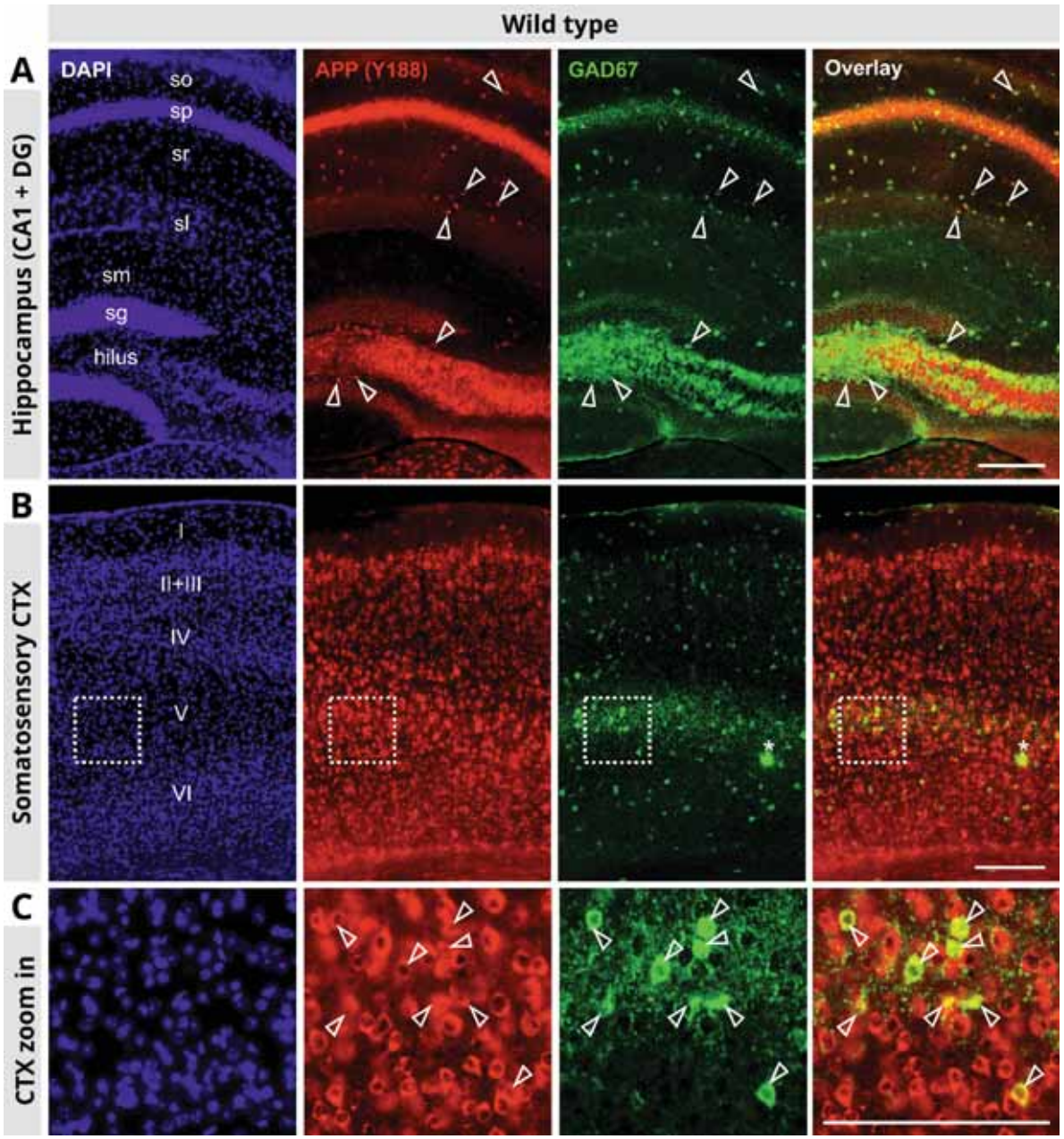
Wild type
A
Hippocampus (CA1 + DG)
DAPI
so
sp
sr
sl
sm
sg
hilus
APP (Y188)
GAD67
Overlay
B
Somatosensory CTX
I
II+III
IV
V
VI
C
CTX zoom in

Figure 1

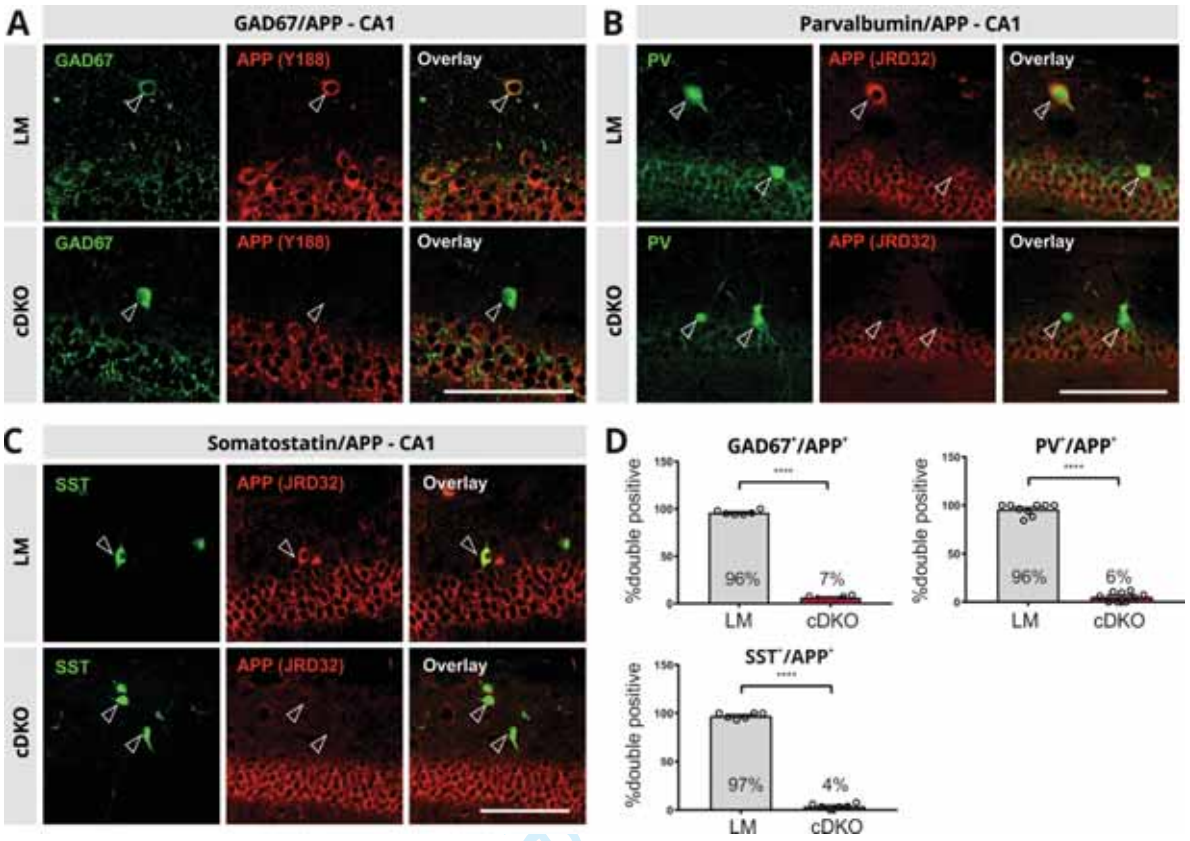

Figure 2

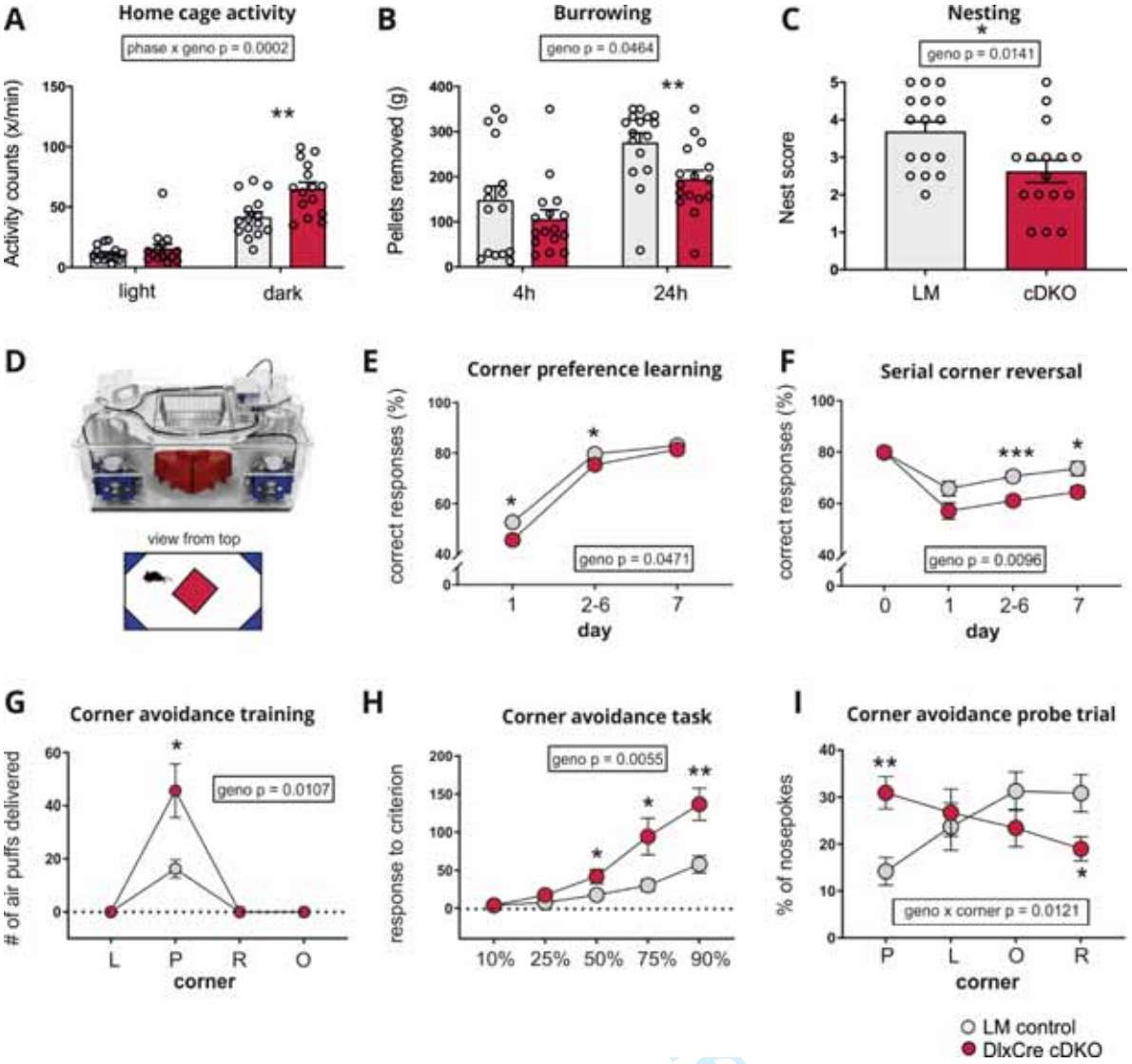
A
Home cage activity
phase x geno p = 0.0002
Activity counts (x/min)
light
dark
B
Burrowing
geno p = 0.0464
Pellets removed (g)
4h
24h
C
Nesting
geno p = 0.0141
Nest score
LM
cDKO
D
view from top
E
Corner preference learning
correct responses (%)
geno p = 0.0471
day
F
Serial corner reversal
correct responses (%)
geno p = 0.0096
day
G
Corner avoidance training
# of air puffs delivered
geno p = 0.0107
corner
H
Corner avoidance task
response to criterion
geno p = 0.0055
I
Corner avoidance probe trial
% of nosepokes
geno x corner p = 0.0121
corner
LM control
DlxCre cDKO

Figure 3

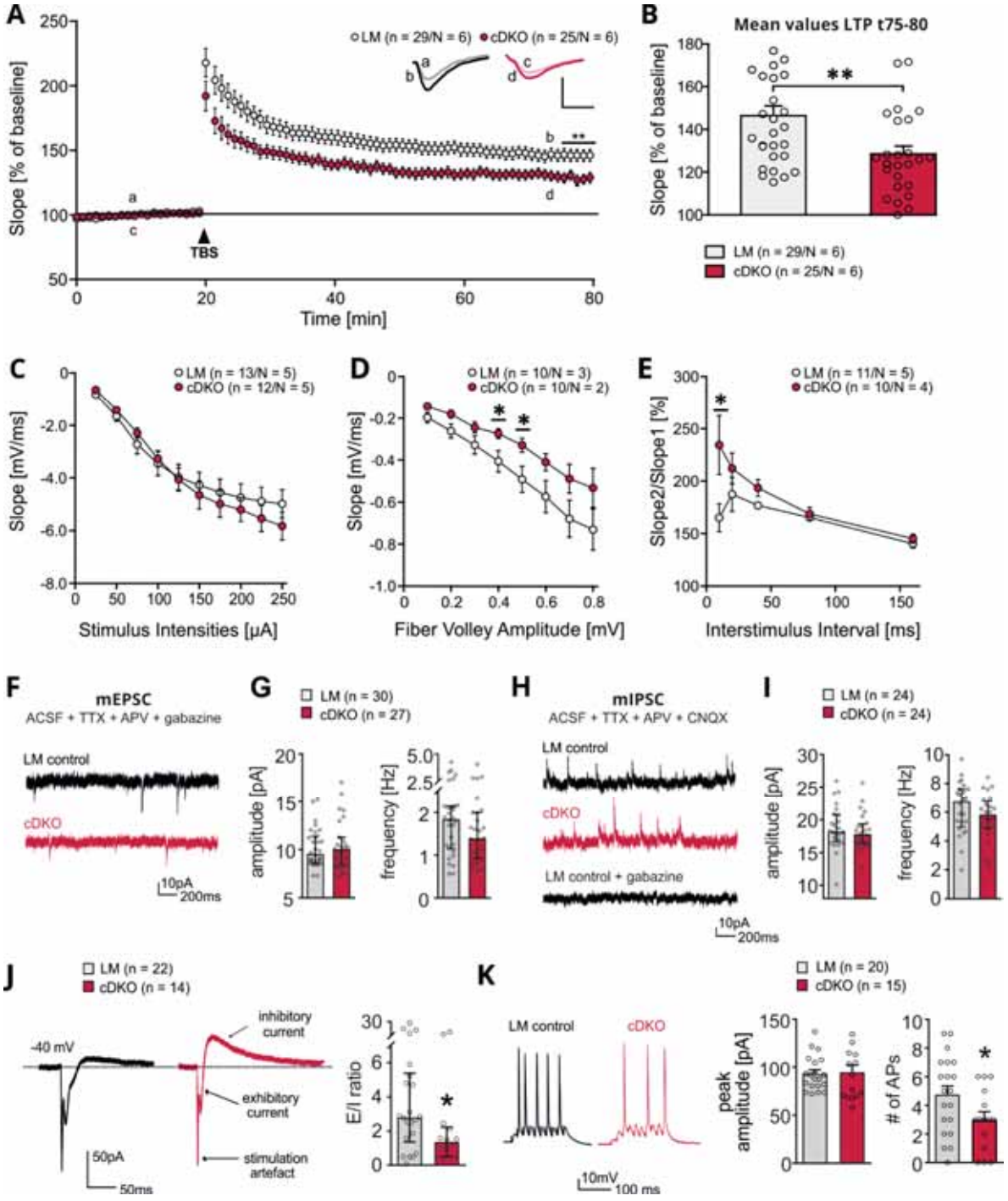
A
LM (n = 29/N = 6)
cDKO (n = 25/N = 6)
Slope [% of baseline]
TBS
Time [min]
B
Mean values LTP t75-80
Slope [% of baseline]
LM (n = 29/N = 6)
cDKO (n = 25/N = 6)
C
LM (n = 13/N = 5)
cDKO (n = 12/N = 5)
Slope [mV/ms]
Stimulus Intensities [µA]
D
LM (n = 10/N = 3)
cDKO (n = 10/N = 2)
Slope [mV/ms]
Fiber Volley Amplitude [mV]
E
LM (n = 11/N = 5)
cDKO (n = 10/N = 4)
Slope2/Slope1 [%]
Interstimulus Interval [ms]
F
mEPSC
ACSF + TTX + APV + gabazine
LM control
cDKO
10pA
200ms
G
LM (n = 30)
cDKO (n = 27)
amplitude [pA]
frequency [Hz]
H
mIPSC
ACSF + TTX + APV + CNQX
LM control
cDKO
LM control + gabazine
10pA
200ms
I
LM (n = 24)
cDKO (n = 24)
amplitude [pA]
frequency [Hz]
J
LM (n = 22)
cDKO (n = 14)
-40 mV
inhibitory current
exhibitory current
stimulation artefact
50pA
50ms
E/I ratio
K
LM (n = 20)
cDKO (n = 15)
LM control
cDKO
10mV
100 ms
peak amplitude [pA]
# of APs

Figure 4

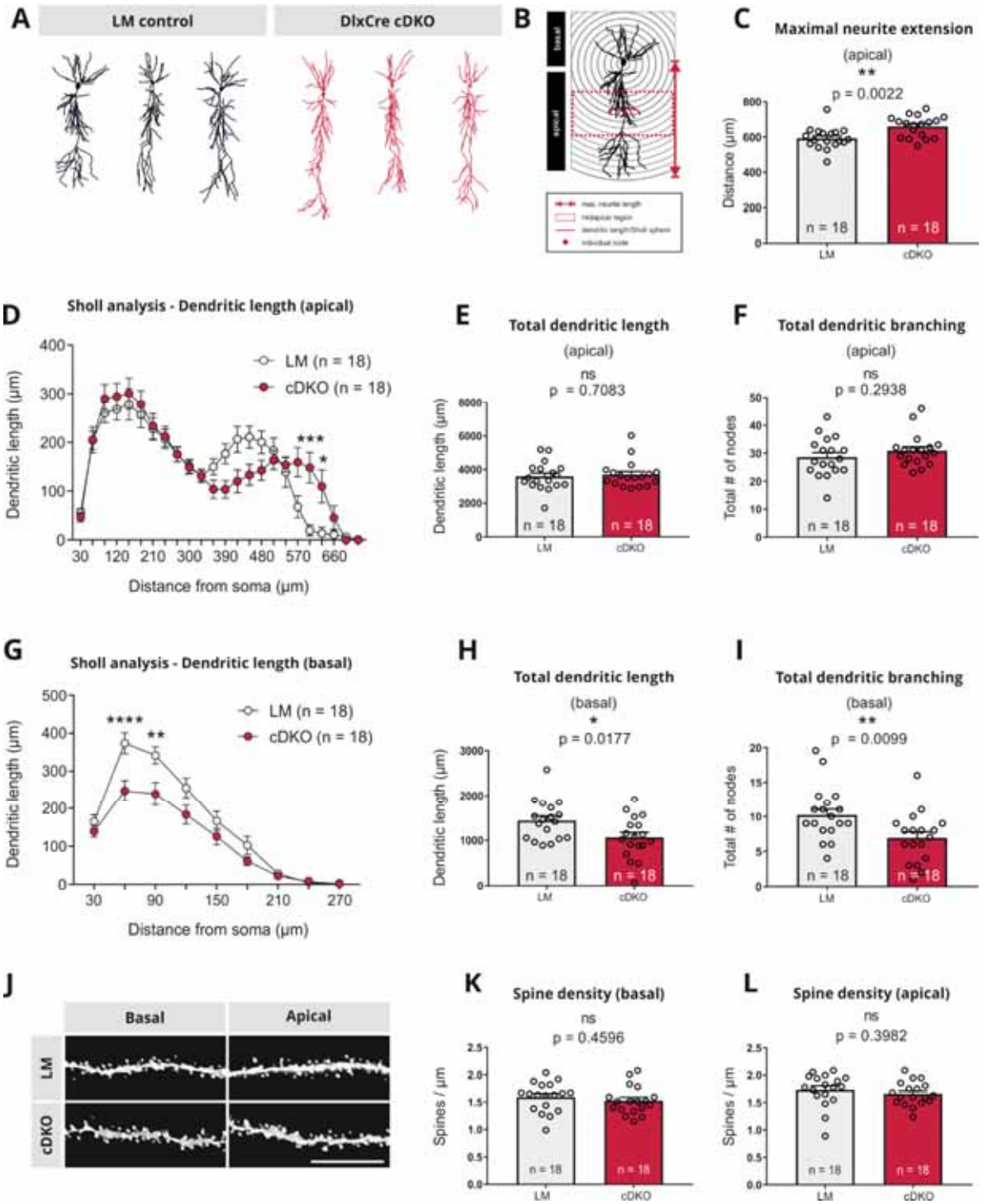
A
LM control
DlxCre cDKO
B
basal
apical
C
Maximal neurite extension
(apical)
**
p = 0.0022
Distance (µm)
n = 18
n = 18
LM
cDKO
D
Sholl analysis - Dendritic length (apical)
LM (n = 18)
cDKO (n = 18)
Dendritic length (µm)
***
*
Distance from soma (µm)
E
Total dendritic length
(apical)
ns
p = 0.7083
Dendritic length (µm)
F
Total dendritic branching
(apical)
ns
p = 0.2938
Total # of nodes
G
Sholl analysis - Dendritic length (basal)
LM (n = 18)
cDKO (n = 18)
****
**
Dendritic length (µm)
Distance from soma (µm)
H
Total dendritic length
(basal)
*
p = 0.0177
Dendritic length (µm)
I
Total dendritic branching
(basal)
**
p = 0.0099
Total # of nodes
J
Basal
Apical
LM
cDKO
K
Spine density (basal)
ns
p = 0.4596
Spines / µm
L
Spine density (apical)
ns
p = 0.3982
Spines / µm

Figure 5

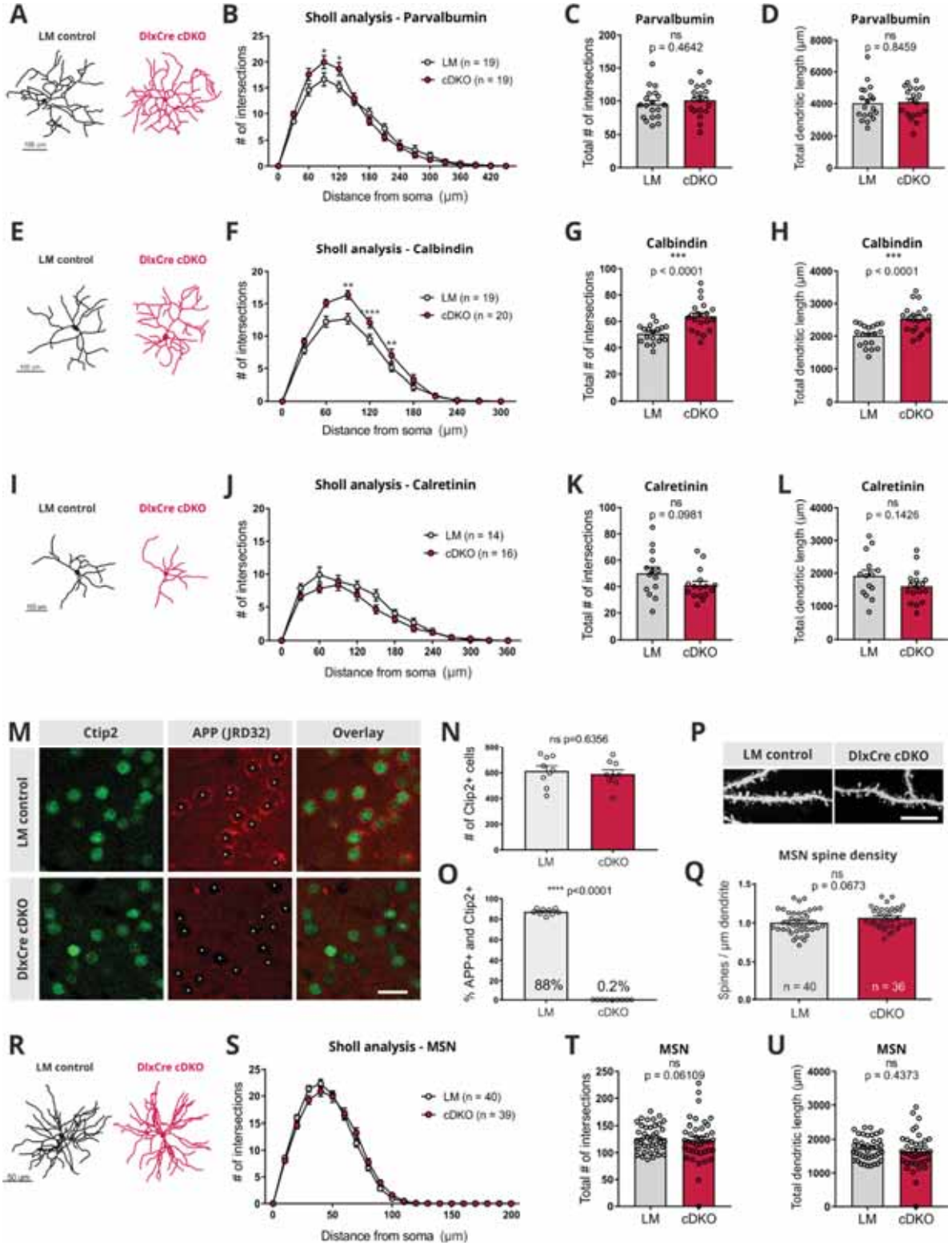
A
LM control
DlxCre cDKO
B
Sholl analysis - Parvalbumin
LM (n = 19)
cDKO (n = 19)
# of intersections
Distance from soma (µm)
C
Parvalbumin
ns
p = 0.4642
Total # of intersections
LM
cDKO
D
Parvalbumin
ns
p = 0.8459
Total dendritic length (µm)
E
LM control
DlxCre cDKO
F
Sholl analysis - Calbindin
LM (n = 19)
cDKO (n = 20)
G
Calbindin
***
p < 0.0001
H
Calbindin
***
p < 0.0001
I
LM control
DlxCre cDKO
J
Sholl analysis - Calretinin
LM (n = 14)
cDKO (n = 16)
K
Calretinin
ns
p = 0.0981
L
Calretinin
ns
p = 0.1426
M
Ctip2
APP (JRD32)
Overlay
LM control
DlxCre cDKO
N
ns p=0.6356
# of Clip2+ cells
O
**** p<0.0001
% APP+ and Clip2+
88%
0.2%
P
LM control
DlxCre cDKO
Q
MSN spine density
ns
p = 0.0673
Spines / µm dendrite
n = 40
n = 36
R
LM control
DlxCre cDKO
S
Sholl analysis - MSN
LM (n = 40)
cDKO (n = 39)
T
MSN
ns
p = 0.06109
U
MSN
ns
p = 0.4373

Figure 6

Supplements

Supplementary Methods

LacZ staining

Sections of fresh-frozen brains from 2-month-old mice (n = 4) were cut with a thickness of 30 µm and thaw-mounted on Superfrost plus microscope slides (Menzel). After drying, slices were postfixed in 0.2% glutaraldehyde in washing solution (5 mM EGTA, 2 mM $MgCl_2$, 0.01% Na-Deoxycholate, 0.02% NP-40 in PBS, pH 7.3) for 5 min and then washed twice in washing solution for 5 min each. Slides were put into the staining solution (washing solution containing 10 mM $K_3[Fe(CN)_6]$, 10 mM $K_4[Fe(CN)_6]$ and 0.5 mg/ml X-Gal in DMF) for 3 to 24 h depending on the desired staining intensity, washed in PBS two times for 5 min each, and mounted in Mowiol. Overview images were obtained on a Nikon Eclipse (Ni-E) upright automated microscope with a 10x objective (Plan Apo 10×/0.45) at the Nikon Imaging Centre (NIC) at the University of Heidelberg.

Western Blotting

Mice (19 weeks old) were euthanized with an overdose of CO_2 and hippocampus and cortex were immediately dissected and frozen in liquid nitrogen. Brain samples were thawed on ice and homogenized for 20 sec using a Polytron PT-MR 2100 homogenizer (Polytron PT-MR 2100, Kinematica AG, Switzerland) and homogenization buffer (THB, 250 mM sucrose, 1 mM EGTA, 20 mM Tris–HCl, pH 7.4) containing 1× protease inhibitor (Complete TM #04693124001, Roche, Switzerland). Homogenates were centrifuged for 10 min at 15700 g and 4°C, supernatants directly used for protein quantification by BCA assay or snap-frozen in liquid nitrogen and stored at –80°C. Brain samples were separated on 10% Tris-Glycin gels (20 µg/lane) at 120V in Laemmli buffer (0.25M Tris, 2M glycine and 1% SDS). Proteins were transferred onto Ø 0.45 µm PVDF membranes (GE Healthcare) which were blocked in PBST (1x PBS + 0.05% Tween-20) + 5% (w/v) skimmed milk powder (MP) at room temperature for

60 min. Membranes were cut as indicated by a dashed line in the figures to allow for incubation of the same membrane with different primary antibodies. Primary antibodies were diluted in PBST + 2% MP and incubated overnight at 4°C. Primary antibodies: APLP1/CT11 (rabbit, 1:1000, Calbiochem, not available), GAPDH (rabbit, 1:5000, #ABS16, Merck, Germany). Incubation with suitable HRP-conjugated secondary antibodies diluted in PBST + 1% MP was for 60 min at room temperature. Secondary antibodies: goat-α-rabbit HRP (1:10.000, #111-035-144, Jackson ImmunoResearch, United Kingdom). Bands were visualized with Fire ECL Reagent (#6883, Cell Signaling Technology, USA) as specified by the manufacturer. Signals were detected with the BioRad ChemiDoc Imager (Bio-Rad, Hercules, USA). Exposure times were chosen in a away that bands contained no saturated pixels, and only then were quantified using the BioRad ImageLab software. After exporting obtained values to Excel, each band was normalized to its corresponding GAPDH band, which served as loading control, and mean values for each genotype were calculated. Statistical analysis of arbitrary units (AU) was done using the two-tailed Student's t-test, level of significance was set at $p<0.05$.

Behavior - Grip strength

Forepaw grip strength was measured as described previously (Ring et al. 2007) using a newton meter (max. force: 300 g) that was positioned horizontally and attached to a metallic ring of 5.5 cm diameter and 3 mm thickness. Mice were held by the tail and allowed to grasp the ring with both forepaws. They were then gently pulled back until they released the ring. Five measurements were obtained each on 2 consecutive days and averaged.

Supplementary Figures

Figure S1. APP expression in cell type-specific conditional NexCre and DlxCre cDKOs mice.

Immunohistochemistry for APP using JRD32 antibody (white) in coronal brain section (40 µm) of **(A)** wild type (WT) mice, **(B)** NexCre cDKO and **(C)** DlxCre cDKO mice. Note the absence of APP immunoreactivity selectively in excitatory forebrain neurons in NexCre cDKOs mice **(A).** In the hippocampus (HC) and cortex (CTX; lager magnification of the boxed area on the left) APP immunoreactivity is absent from principal cells leading to a sparse pattern of APP^+ cells consistent with APP expression in interneurons. In DlxCre cDKOs staining intensity is weaker in the striatum (whole brain image) and cortex (CTX, **C**). Whereas in WT hippocampus (HC) a considerable number of APP^+ cells can be found outside of the pyramidal cell bundle **(A)** and this cell population is absent in DlxCre cDKOs that express Cre in GABAergic forebrain neurons **(C)**. Representative images from n = 3 animals/genotype (age: 5-month-old). Scale bars whole brain: 500 µm; HC and CTX: 300 µm.

Figure S2. Hippocampal APP+ cells in NexCre cDKO mice are GABAergic interneurons.

Immunohistochemistry for APP and interneurons markers in hippocampal layers of NexCre cDKOs mice. Coronal sections (40µ) were stained for APP (JRD32; red) and the interneuron marker parvalbumin (PV; green), somatostatin (SST; green) or calretinin (CR, green) to assess the cell type of APP^+ cells in NexCre cDKO mice. DAPI staining (left panel) indicates cell nuclei in blue **(A)** A proportion of APP^+ cells in the stratum oriens (so), the pyramidal cell bundle (CA1) and the DG are PV^+ interneurons as evidenced by overlapping immunoreactivity. Exemplary APP^+/PV^+ cells are indicated by arrowheads. **(B)** SST^+ cells in stratum oriens (so) or the hilus of the DG are double positive for APP (white arrowheads). **(C)** A proportion of APP^+ cells in the pyramidal CA1 bundle and stratum lacunosum moleculare (slm) in CA1 and

in the hilus (DG) are CR^+ interneurons (white arrowheads). Representative confocal images of 3 animals/genotype (age: 5-month-old). So = stratum oriens, sp = stratum pyramidale, sr = stratum radiatum, slm = stratum lacunosum moleculare, sm = stratum moleculare and sg = stratum granulosum. Scale bars (A, B, C): 300 µm.

Figure S3. Validation of Cre expression in DlxCre mice crossed with Cre reporter mouse lines.

Cre recombinase expression in DlxCre animals was monitored by crossing them with reporter mice. (**A, B**) Schematic representation of the ROSA26 reporter locus in Ai14 (**A**) and ROSA26/lacZ mice (**B**) tdTomato or LacZ are expressed under the control of the ubiquitous and constitutive ROSA26 promoter. After Cre-mediated recombination, the floxed STOP-cassette in front of the tdTomato (**A**) or LacZ gene (**B**) is excised, which leads to tdTomato (red fluorescence) or β-galactosidase expression, respectively. (**C**) Sagittal brain sections (40 µm) from $DlxCre^{+/T}$ $Ai14^{+/T}$ and LacZ-stained $DlxCre^{+/T}$ $ROSA26LacZ^{+/T}$ reporter animals indicate Cre activity due to tdTomato expression (red) or after LacZ staining (blue). Prominent Cre activity was detected in the striatum (CP, caudate putamen), in the hypothalamus (HY) and in the main olfactory bulbs (MOB). In addition, $DlxCre^{+/T}$ $Ai14^{+/T}$ reporter mice show strong tdTomato expression in the substantia nigra (SN). In the hippocampal formation (HPF) and cortex (CTX) Cre^+ cells were identified as a sparse population, as expected for interneurons. Prominent Cre activity in the striatum is due to Cre expression in GABAergic medium spiny neurons. No or only very few Cre positive cells were detected in other brain regions, including the thalamus (TH) and the cerebellum (CBX). Representative images from n = 5 animals/genotype (age: 1.6-2-month-old). Note, that the depicted LacZ-stained section is more lateral compared to the $DlxCre^{+/T}$ $Ai14^{+/T}$ section and does not contain the substantia nigra (SN). Scale bars whole brain: 1 mm; HC, CTX, CP: 200 µm.

Figure S4. Cre recombinase is expressed in major interneuron subsets in the hippocampus of DlxCre mice.

(A, B) Coronal brain sections (40 µm) of DlxCre$^{+/T}$ Ai14$^{+/T}$ mice were stained against the interneuron marker GAD67 (green), parvalbumin (PV; green) or calretinin (CR; green) to assess the percentage of Cre/tdTom^{+} (red) GABAergic cells in all hippocampal subfields (CA1, CA3, and DG). **(C)** Most GAD67^{+} interneurons (CA1: 95.06%; CA3: 96.17%) express tdTomato (red) indicating efficient expression of Cre recombinase in GABAergic cells of DlxCre cDKO mice. Similarly, almost all PV^{+} interneurons in the hippocampal subfields CA1, CA3 or DG (> 94.00%) express tdTomato (red). Moreover, most CR^{+} interneurons (83.44 – 92.92%) express Cre recombinase as indicated by tdTomato expression (red). Representative images of n = neurons from 5 animals (age: 2 month-old) and 9 sections/genotype. Error bars indicate ± SEM. Scale bars (A): 100 µm; (B): 200 µm.

Figure S5. APP is efficiently deleted in major interneuron subsets of the CA3 and DG regions of DlxCre cDKO hippocampus while the total number of major interneuron subtypes in the hippocampus is normal.

(A, C, E) Coronal brain sections (40 µm) of DlxCre cDKOs and littermate (LM) control mice were stained against APP (JRD32 or Y188, red) and the interneuron markers GAD67 (green), parvalbumin (PV; green) or somatostatin (SST; green) to assess the APP knockout efficiency in the CA3, and DG hippocampal subfields. For knockout efficiency in CA1 see Fig. 2. **(B)** Most GAD67^{+} interneurons (double-positive in CA3: 96%) express APP (Y188 staining) in LM control mice but not in DlxCre cDKOs (double-positive in CA3: 7%), indicating an efficient APP KO in GABAergic cells. **(D)** Similarly, most PV^{+} interneurons (double-positive in CA3: 93%; DG: 100%) express APP (JRD32 staining) in LM controls but not in DlxCre

cDKOs (double-positive in CA3: 5%; DG: 2%). **(F)** In line, most SST^+ interneurons (double-positive in CA3: 96%; DG: 98%) express APP (JRD32) in LM control mice but not in DlxCre cDKOs (double-positive in CA3: 1%; DG: 2%). Unpaired Student's t-test, n = 6–9 sections, ****p < 0.0001. **(G)** The number of $GAD67^+$, PV^+ or SST^+ cells was comparable between genotypes (Unpaired Student's t-test, n (sections) = 6-9, ns = not significant), indicating that the cDKO does not affect interneuron formation or survival. Representative confocal images of 3 animals/genotype (age: 4-month-old). Error bars indicate ± SEM. Scale bars (A, C, E): 200 µm.

Figure S6. Western blot analysis of APLP1 expression in DlxCre cDKO tissue and interneurons.

(A-D) Western blot analysis of APLP1 expression with APLP1-specific CT11 antibody in cortex **(A,B)** and hippocampus (HC; **C,D)** of LM control (N = 6) and DlxCe cDKO mice (N = 6). Age of mice: 4-5 months**. (B, D)** Quantification of APLP1 expression in cortex (CTX; **B)** and HC **(D)** normalized to GAPDH levels. Note, that expression of APLP1 in DlxCre cDKO and LM mice is comparable. Error bars indicate ± SEM. Data were analyzed by unpaired Student's t-test, two-tailed, N (animals) = 6, p = 0.41 or 0.52, ns = not significant. **(E, F)** Analysis of APLP1 expression (red) in interneurons (green) *in vitro*. **(E)** Interneurons were identified by EGFP expression upon transducing primary hippocampal cultures with AAV-mDlx-EGFP-Fishell-1 at DIV7. **(F)** Mean Intensity Fluorescence (MFI) of APLP1 immunoreactivity was quantified at DIV14 in EGFP+ somata and normalized to the analyzed area using ImageJ (Fiji). Note, that no significant difference was detectable in DlxCre cDKO interneurons as compared to LM cells. Data were analyzed by unpaired Student's t-test, two-tailed, n (neurons) = 18, p = 0.54, ns = not significant. Analysis was performed blind to genotype.

Figure S7. Motor function of DlxCre cDKOs is normal.

(A) Grip strength: Grip strength was assessed during two sessions (A & B) for 5 trials each. There was no effect of the APP/APLP2 cDKO on grip strength (geno $F(1,28) = 0.7$ ns; session $F(1,28) = 3.3$ $p < 0.0812$; session x geno $F(1,28) = 0.09$ ns). N = 15 (animals)/genotype. Sex: 7 males, 8 females per genotype. **(B) Rotarod**: Time to fall during 5 trials of training on the accelerating rotarod (4-40 rpm in 300s). Neither level nor time course of performance were affected in DlxCre cDKOs (geno $F(1,28) = 0.5$ ns; trial $F(4,112) = 3.1$ $p < 0.0195$; trial x geno $F(1,28) = 0.04$ ns). N = 15 (animals)/genotype. Sex: 7 males, 8 females per genotype. Date are represented as mean ± SEM. Data were analyzed using mixed ANOVA models with genotype (DlxCre cDKO vs. littermate (LM) control) as between subject factor and within subject factors to explore the dependence of genotype effects on place, time, or stimulus. Significant interactions and where necessary significant main effects were further explored by Tukey-Kramer post-hoc tests or by splitting the ANOVA model, as appropriate. One-sample t-tests were used for follow-up comparisons against chance levels. The significance threshold was set at 0.05. The false discovery rate (FDR) control procedure of Hochberg was applied to groups of conceptually related variables within single tests to correct significance thresholds for multiple comparisons. *$p < 0.05$, **$p < 0.01$, ***$p < 0.001$.

Figure S8. IntelliCage apparatus and task paradigms.

(1) Overview of the IntelliCage apparatus: The IntelliCage (IC) fits inside a large housing cage and provides four recording chambers in the four corners of the cage (indicated by blue triangles). The IntelliCage is a computer-based, fully automated testing apparatus used to analyze the spontaneous behavior and learning of groups of radiofrequency (RF) ID-tagged mice in a home cage (for further details see Endo et al. 2011). Female mice were group-housed

(always mixed genotypes) and their behavioral responses (corner visits, nose pokes, and lickings) were monitored in a fully automated manner. The tubular RFID reader can record an implanted ID number (transponder) when a mouse visits a corner (e.g. for nose poking) where it can receive water as a reward. Photo beams record the nose pokes of the mice and the holes can be closed by small motorized doors, thus barring access to the water bottles in each corner. Four triangular red shelters (indicated by a red square; Tecniplast, Buguggiate, Italy) were placed in the middle of the IntelliCage. They were used as sleeping quarters and as a stand to reach the food. The IntelliCage was controlled by a computer with dedicated software (IntelliCage Plus), executing pre-programmed experimental schedules. The number and duration of the following behavioral parameters were recorded: visits to the corner chambers, nose pokes to the doors, and contacts with the bottle (licks).

(2) Free adaptation: The mixed groups of DlxCre cDKO and littermate (LM) control mice were released into the IntelliCage with all doors continuously open. During adaptation (day 1-4) the mice could habituate to the novel environment and learned to visit the corners for obtaining water.

(3) Nose poke adaptation: At the beginning of this phase all doors were closed and the first nose poke of every visit opened the door for 5 seconds. In order to drink more, the mice had to leave the corner and enter again. This phase lasted for 7 days. Performance on day 7 was used as the baseline for active corner avoidance conditioning.

(4) Adaptation to drinking sessions: This phase lasted for 7 days and was similar to the previous one but water was available only in two 1 h sessions during the dark phase (starting 3 h (at 11 h) and 8 h (at 16 h) after the beginning of the dark phase, respectively). Thus, the mice were on water deprivation schedule and developed an increased motivation to visit the corners during specified sessions. Corner preference learning was carried out in drinking sessions, where the percentage of correct visits provides a measure of learning.

(5) Corner preference learning: One correct corner where the doors could be opened by nose poking during the sessions was randomly assigned for each animal (3-4 mice at each corner). The nose pokes in the other 3 corners were not rewarded. This test took 7 days.

(6) Random serial corner reversal: The correct corner was randomly changed at the beginning of each drinking session to a corner different from the one previously learned and rewarded. This test took 7 days.

(7) Nose poke adaptation was repeated as described in (3) and lasted for 5 days.

(8) Passive corner avoidance conditioning: After nose poke adaptation one corner was randomly selected for each animal for passive avoidance conditioning lasting for 24h. No more than 4 animals were assigned to one corner. In the assigned corner, the nose poke triggered an air-puff (~0.8 bar, continuous air-puff, until the animal left the corner) and the doors in this corner remained closed. In all other corners, the first nose poke opened the door for 5 seconds. During training, the nose pokes of every animal are recorded and performance determined as the number of responses in non-punished corners/total responses. Animals received training until they did not improve any further.

(9) Home cage adaptation: After conditioning, animals were carefully removed from the IntelliCages and placed into their standard home cages. An effort was made not to displace the bedding and shelter in the IntelliCage. Mice were deprived of water for the last 18h (of the 24 h) in their home cage until returned to the IC for the air puff corner avoidance probe trial.

(10) Passive corner avoidance probe trial: The water-deprived mice were returned to their IntelliCages for the probe trial and their behavior was monitored for 24 h. The protocol was similar to the nose poke adaptation in (3), i.e. in all corners, the first nose poke opened the door for 5 s.

Figure S9. Impairment of LTP in single DlxCre cKO mice is age-dependent.

(A, B) Adult DlxCre cKO mice (age: 3-4 months) revealed unaltered LTP. TBS induction resulted in comparable potentiation levels of 139 ± 4.8% (WT controls, open circles) and of 135 ± 4.2 % for the final 5 min of LTP for DlxCre cKO slices (black circles; t75-80; unpaired Student´s t-test p = 0.568, ns = not significant). Input-output strength at given stimulus intensities **(C)** or defined fiber volley amplitudes **(D)** were not significantly changed. **(E, F)** After 20 min of baseline recording TBS (arrow) induced a robust and stably maintained LTP in 12 month old WT controls (142 ± 6.1 %, open circles), while age-matched DlxCre cKOs revealed significantly impaired LTP (125 ± 3.2 %, black circles, t75-80; unpaired Student´s t-test, *p = 0.048). **(G, H)** Input-output strength was affected neither at given stimulus intensities nor at defined fiber volley amplitudes. Insets show original traces of representative individual experiments Insets show original traces of representative individual experiments. Vertical scale bar = 1 mV, horizontal scale bar = 5 ms. Error bars indicate ± SEM. n = number of slices. N = number of mice used (adult: 3 to 4-month-old; aged: 12 month-old).

Figure S10. DlxCre cDKO mice show no signs of abnormal astrogliosis or microgliosis.

Sagittal and coronal sections (40 µm) from littermate (LM) control and DlxCre cDKO brains were stained in parallel for GFAP (astroglia marker) or Iba1 (microglia marker). **(A)** Staining intensity and distribution of $Iba1^+$ microglia (green) is comparable between genotypes in hippocampus (HC), cortex (CTX) or striatum (CP). **(B)** No difference in immunoreactivity against GFAP, nor signs of reactive astrogliosis was detectable in hippocampus (HC), cortex (CTX) or striatum (CP) of DlxCre cDKO mice. More intense staining e.g. at the hippocampal fissure is due to staining of astrocytes participating in the formation of the blood-brain barrier at blood vessels (indicated by white arrowheads). Representative images of 3 animals/genotype (age: 4-month-old). Scale bar (A): 300 µm; (B) HC & CTX: 400 µm; CP: 200 µm.

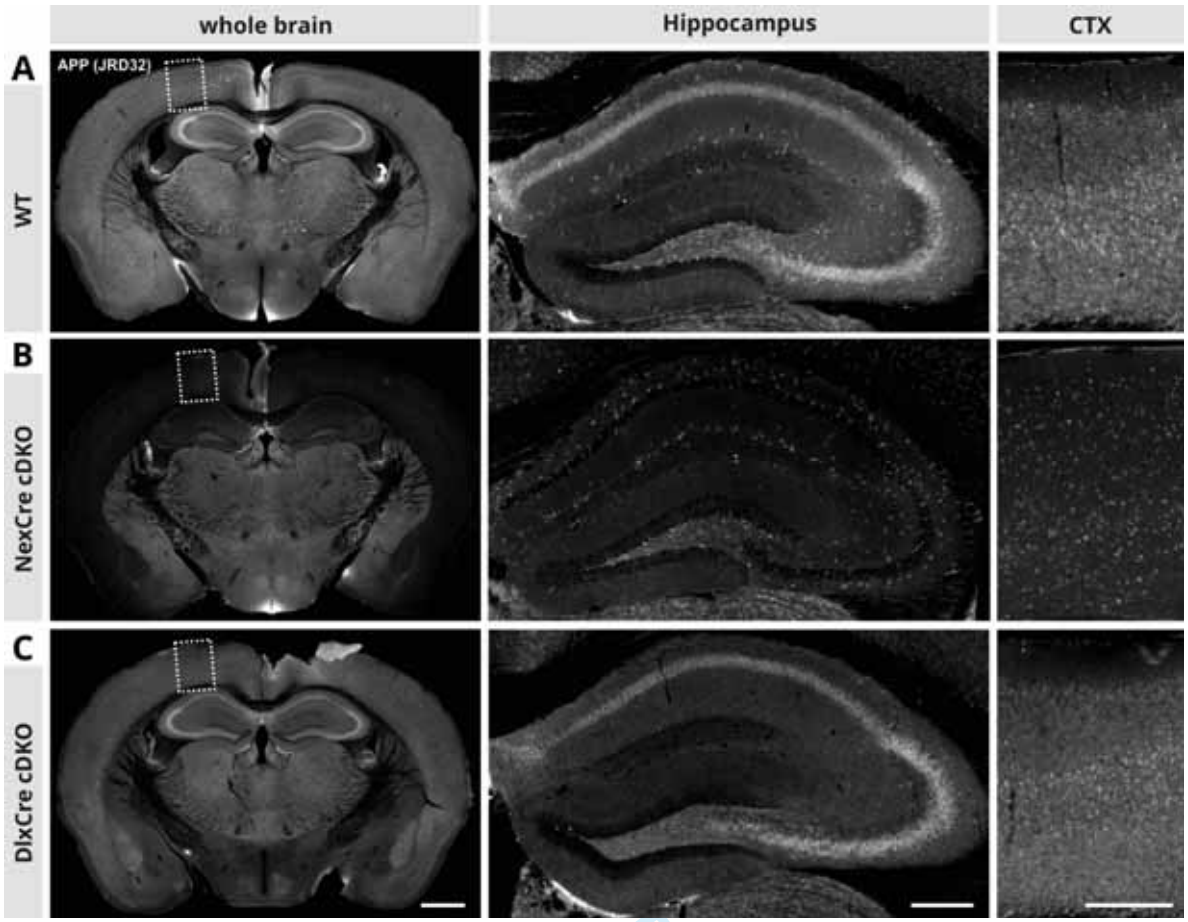

Figure S1

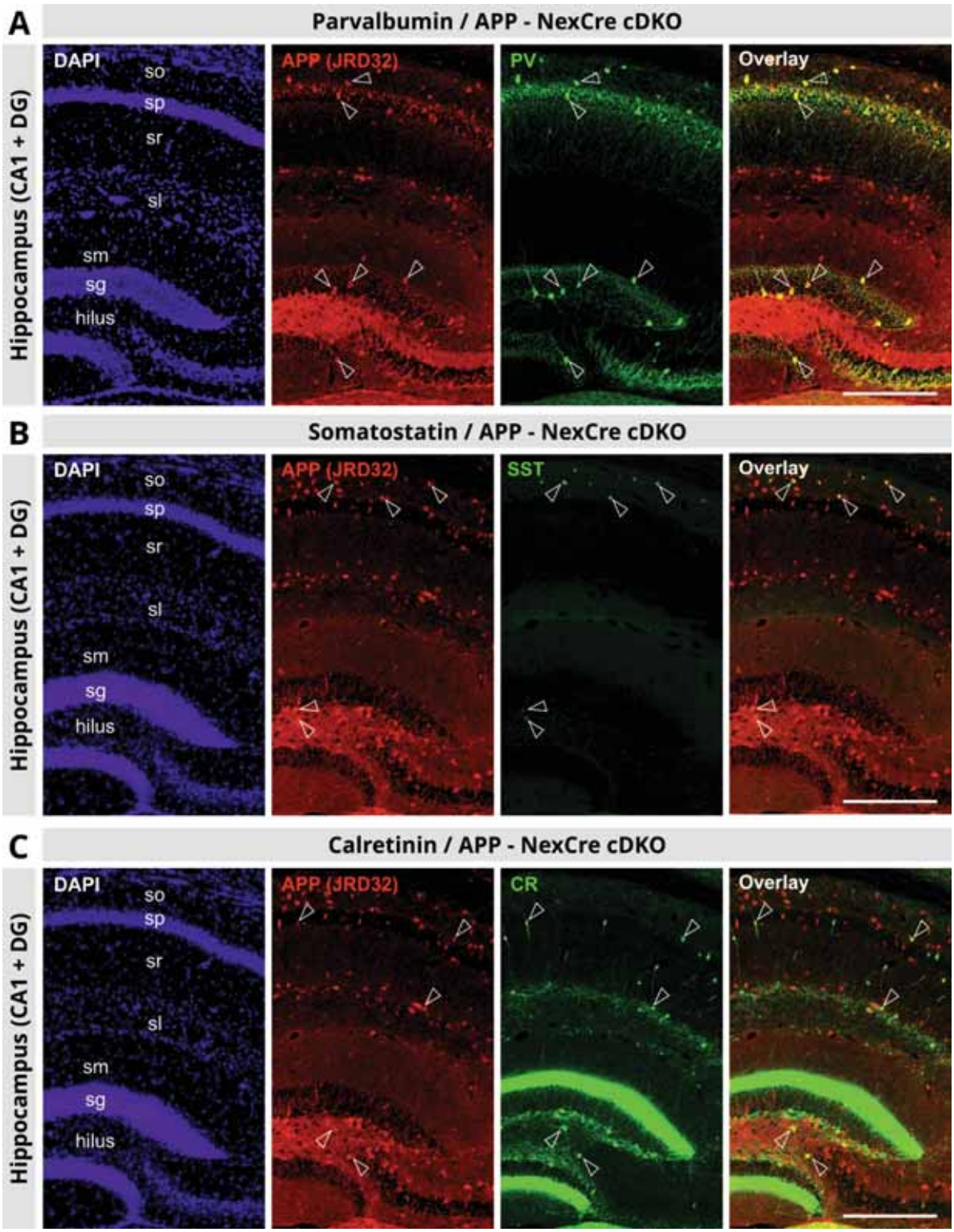
A
Parvalbumin / APP - NexCre cDKO
Hippocampus (CA1 + DG)
DAPI
so
sp
sr
sl
sm
sg
hilus
APP (JRD32)
PV
Overlay
B
Somatostatin / APP - NexCre cDKO
Hippocampus (CA1 + DG)
DAPI
so
sp
sr
sl
sm
sg
hilus
APP (JRD32)
SST
Overlay
C
Calretinin / APP - NexCre cDKO
Hippocampus (CA1 + DG)
DAPI
so
sp
sr
sl
sm
sg
hilus
APP (JRD32)
CR
Overlay

Figure S2

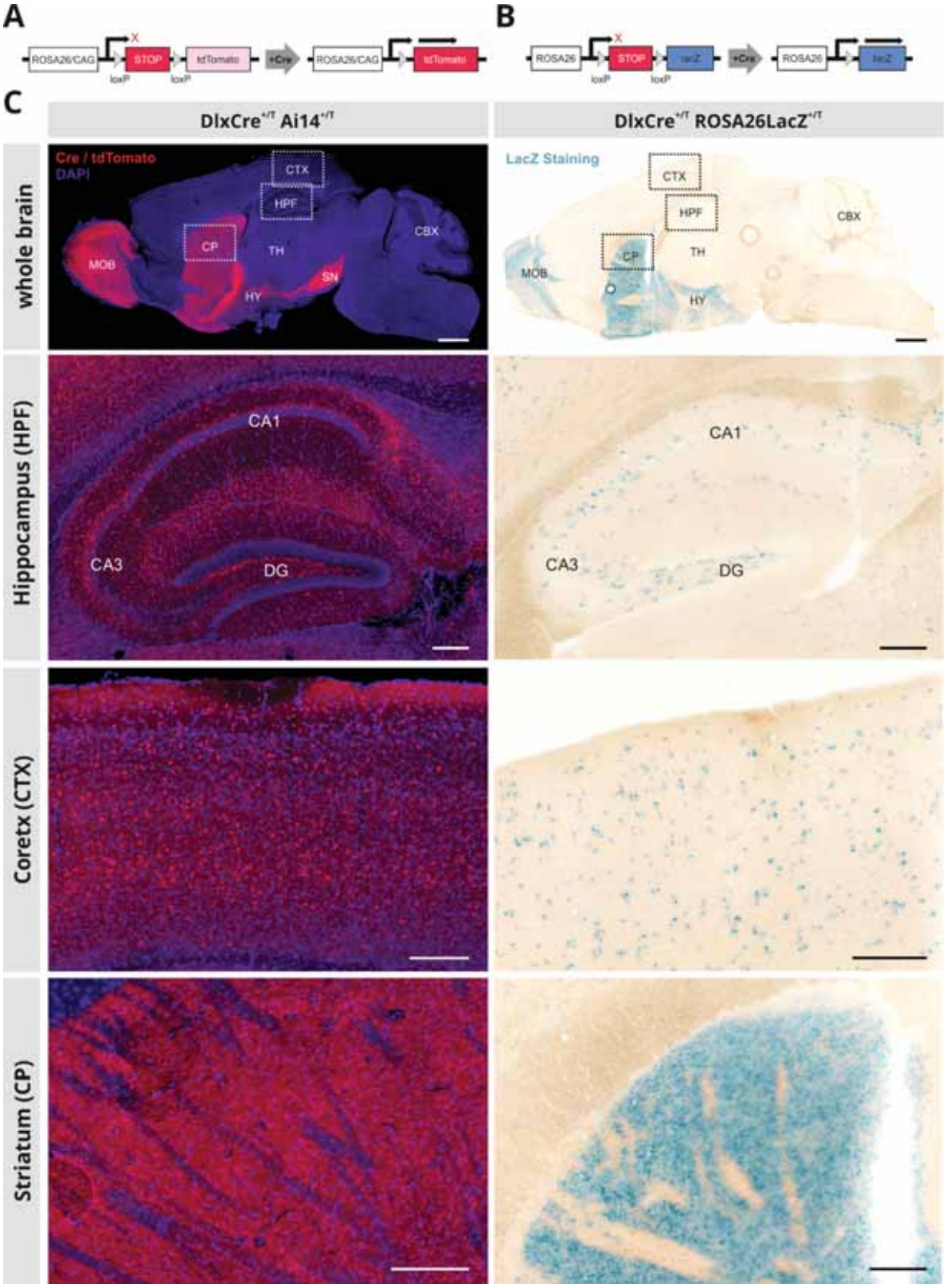
A
ROSA26/CAG
X
STOP
loxP
loxP
tdTomato
+Cre
ROSA26/CAG
tdTomato
B
ROSA26
X
STOP
loxP
loxP
lacZ
+Cre
ROSA26
lacZ
C
DlxCre+/T Ai14+/T
DlxCre+/T ROSA26LacZ+/T
whole brain
Cre / tdTomato
DAPI
CTX
HPF
CP
TH
CBX
MOB
SN
HY
LacZ Staining
CTX
HPF
CBX
CP
TH
MOB
HY
Hippocampus (HPF)
CA1
CA3
DG
CA1
CA3
DG
Coretx (CTX)
Striatum (CP)

Figure S3

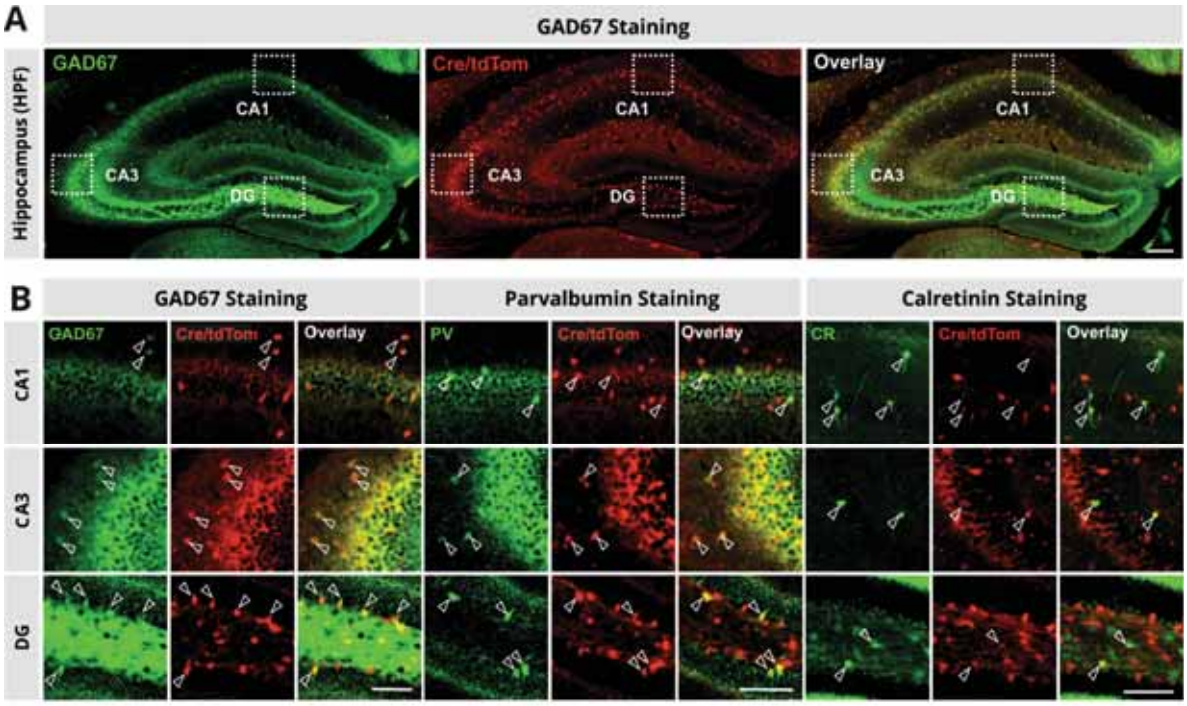

C

HPF subfield	% GAD67+ & Cre/tdTom+ (n)	% PV+ & Cre/tdTom+ (n)	% CR+ & Cre/tdTom+ (n)
CA1	96.17 ± 0.86 (521)	94.08 ± 1.28 (185)	92.92 ± 2.96 (116)
CA3	95.06 ± 1.43 (243)	94.71 ± 1.81 (139)	91.56 ± 5.18 (33)
DG	-	94.16 ± 2.66 (70)	83.44 ± 3.49 (41)

Figure S4

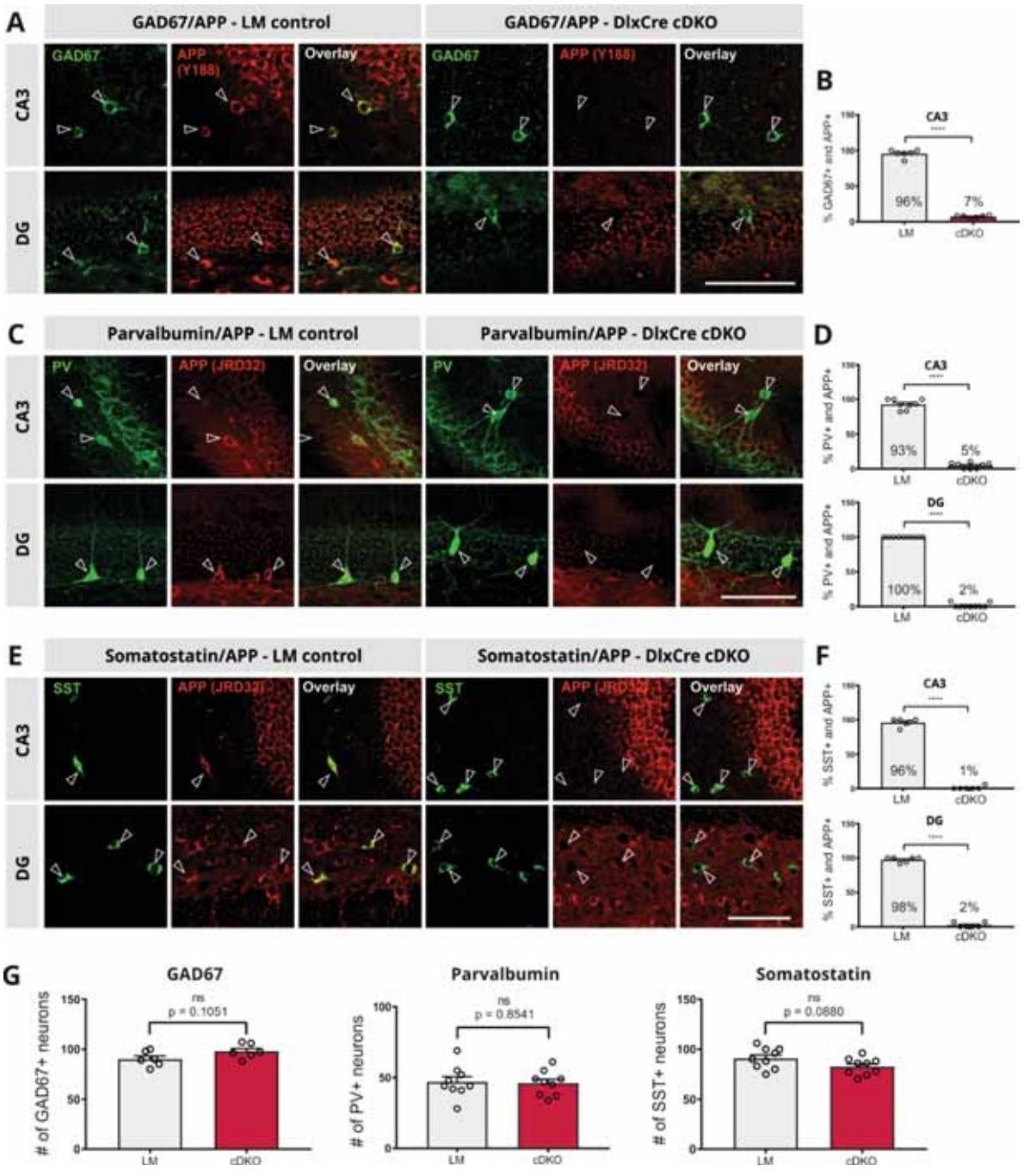
A
GAD67/APP - LM control
GAD67/APP - DlxCre cDKO
CA3
DG
GAD67
APP (Y188)
Overlay
B
CA3
% GAD67+ and APP+
96%
7%
LM
cDKO
C
Parvalbumin/APP - LM control
Parvalbumin/APP - DlxCre cDKO
PV
APP (JRD32)
D
% PV+ and APP+
93%
5%
DG
100%
2%
E
Somatostatin/APP - LM control
Somatostatin/APP - DlxCre cDKO
SST
F
% SST+ and APP+
96%
1%
98%
2%
G
GAD67
Parvalbumin
Somatostatin
# of GAD67+ neurons
# of PV+ neurons
# of SST+ neurons
ns
p = 0.1051
p = 0.8541
p = 0.0880

Figure S5

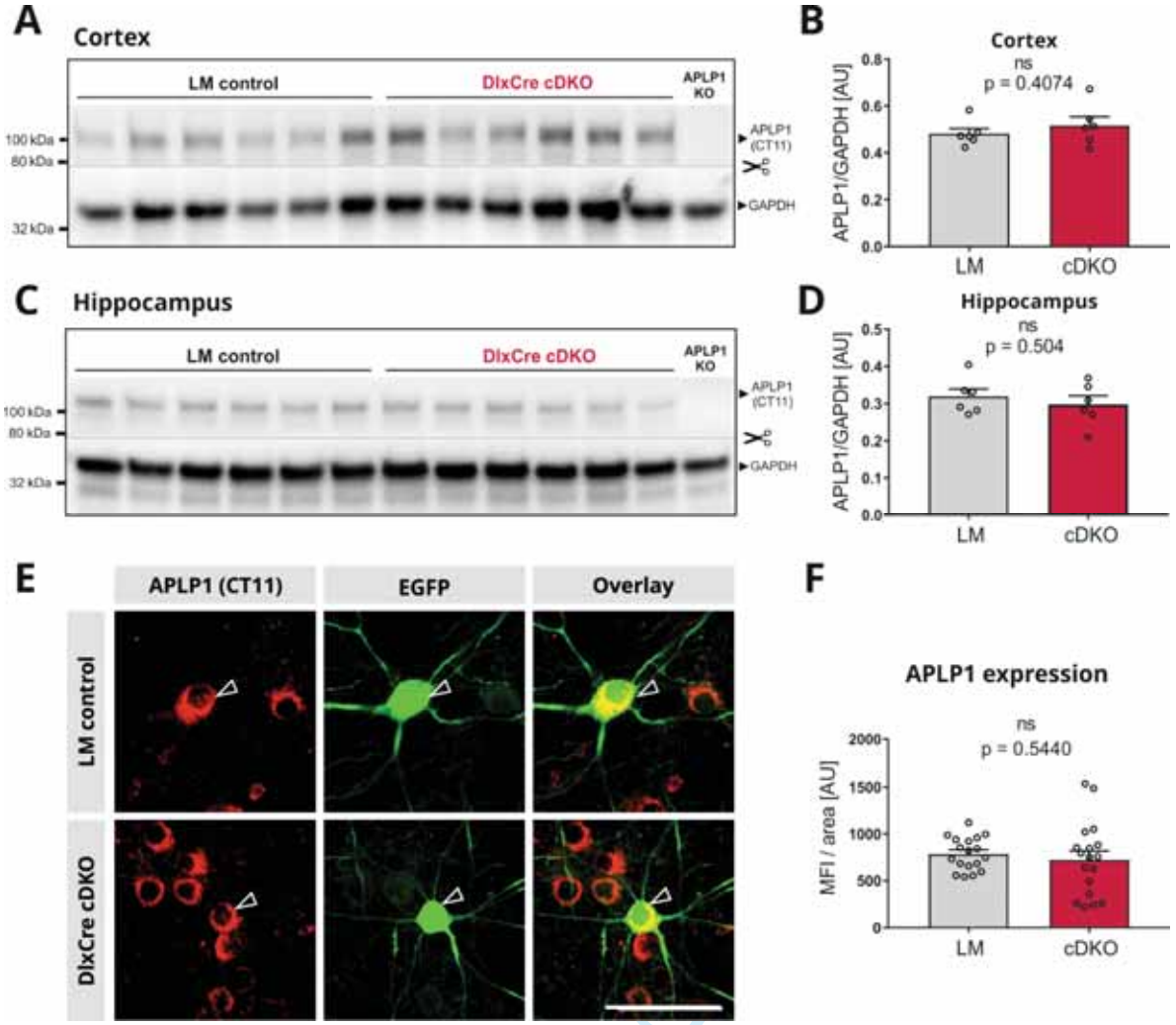

Figure S6

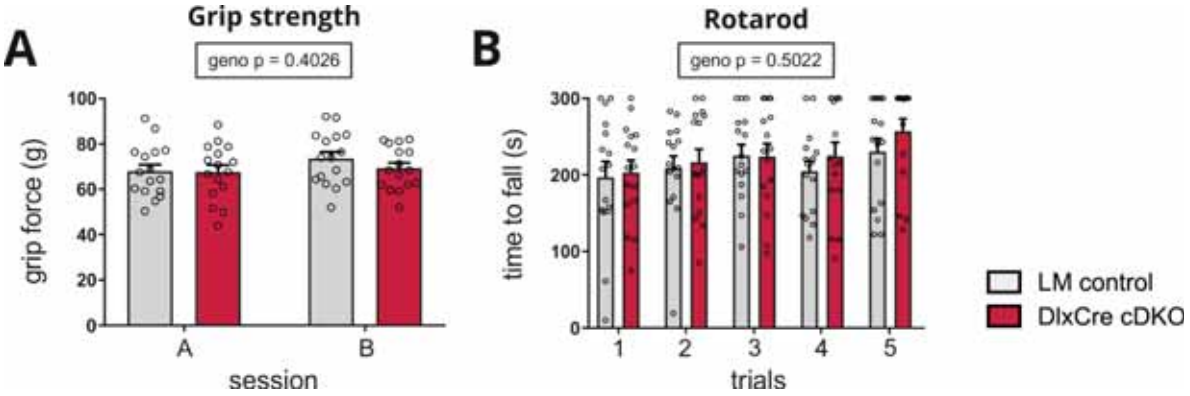

Figure S7

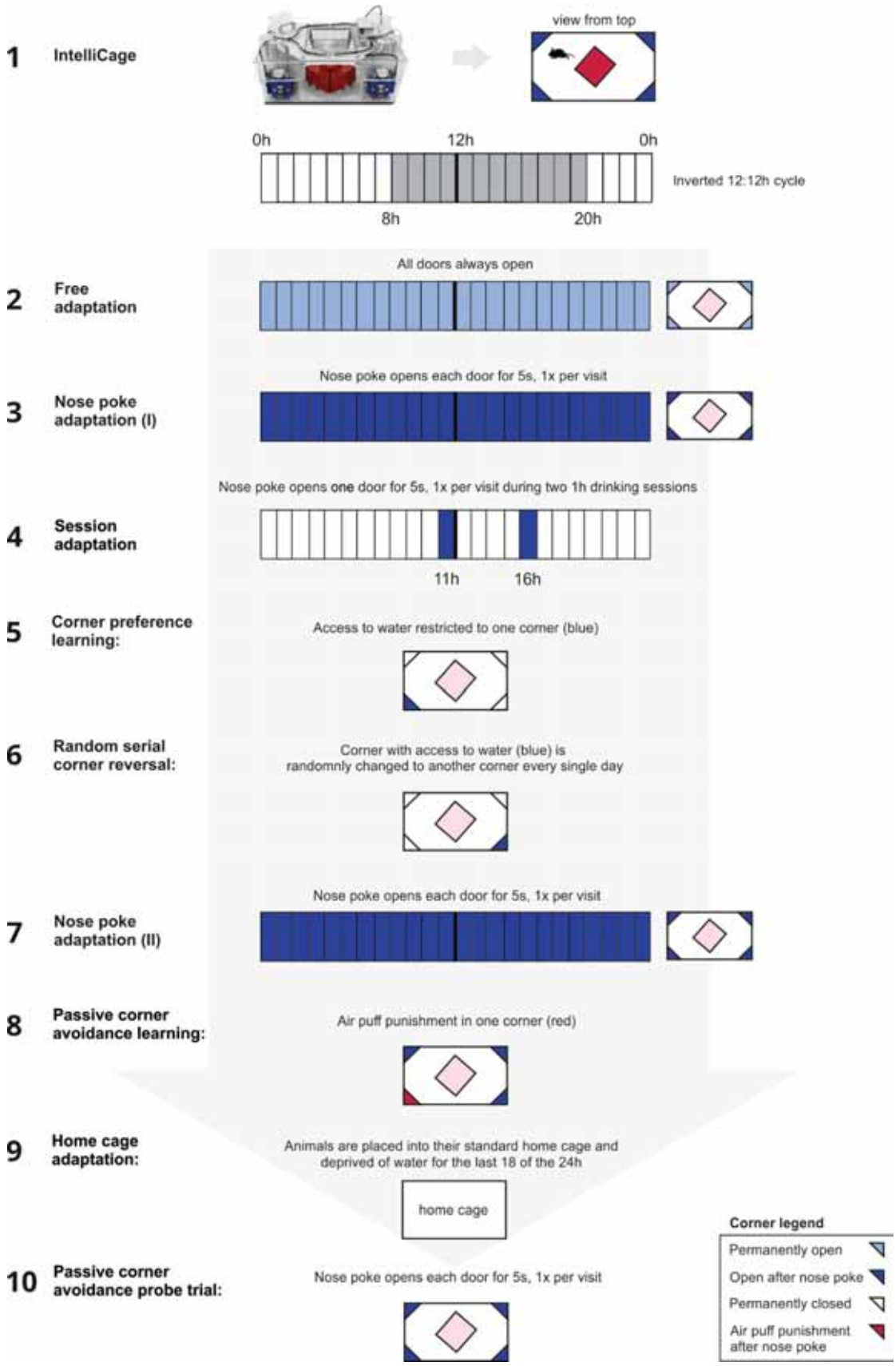
1
IntelliCage
view from top
0h
12h
0h
Inverted 12:12h cycle
8h
20h
2
Free adaptation
All doors always open
3
Nose poke adaptation (I)
Nose poke opens each door for 5s, 1x per visit
4
Session adaptation
Nose poke opens one door for 5s, 1x per visit during two 1h drinking sessions
11h
16h
5
Corner preference learning:
Access to water restricted to one corner (blue)
6
Random serial corner reversal:
Corner with access to water (blue) is randomnly changed to another corner every single day
7
Nose poke adaptation (II)
Nose poke opens each door for 5s, 1x per visit
8
Passive corner avoidance learning:
Air puff punishment in one corner (red)
9
Home cage adaptation:
Animals are placed into their standard home cage and deprived of water for the last 18 of the 24h
home cage
10
Passive corner avoidance probe trial:
Nose poke opens each door for 5s, 1x per visit
Corner legend
Permanently open
Open after nose poke
Permanently closed
Air puff punishment after nose poke

Figure S8

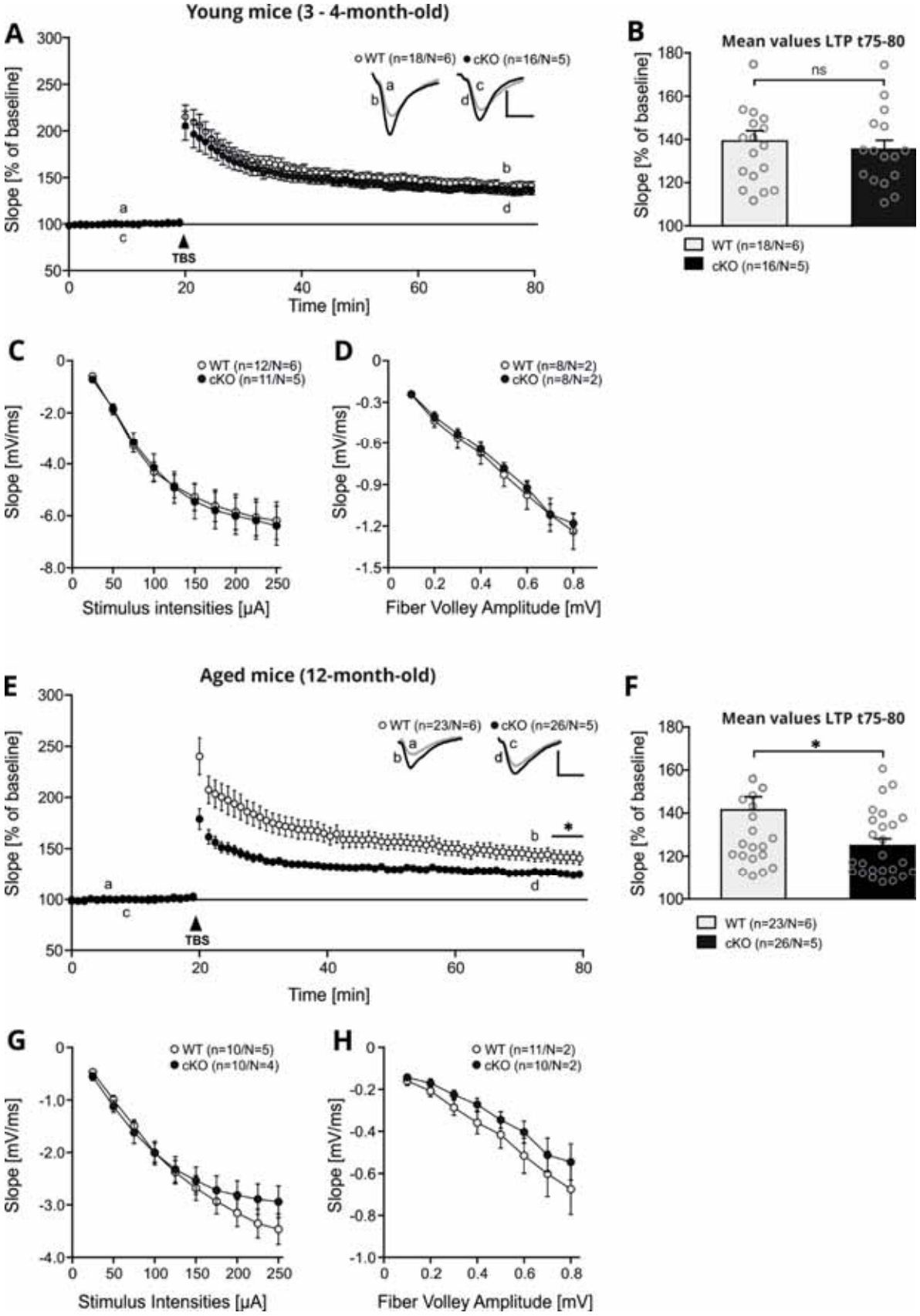
Young mice (3 - 4-month-old)
A
Slope [% of baseline]
WT (n=18/N=6)
cKO (n=16/N=5)
TBS
Time [min]
B
Mean values LTP t75-80
ns
C
WT (n=12/N=6)
cKO (n=11/N=5)
Slope [mV/ms]
Stimulus intensities [µA]
D
WT (n=8/N=2)
cKO (n=8/N=2)
Fiber Volley Amplitude [mV]
Aged mice (12-month-old)
E
WT (n=23/N=6)
cKO (n=26/N=5)
F
Mean values LTP t75-80
*
G
WT (n=10/N=5)
cKO (n=10/N=4)
Stimulus Intensities [µA]
H
WT (n=11/N=2)
cKO (n=10/N=2)

Figure S9

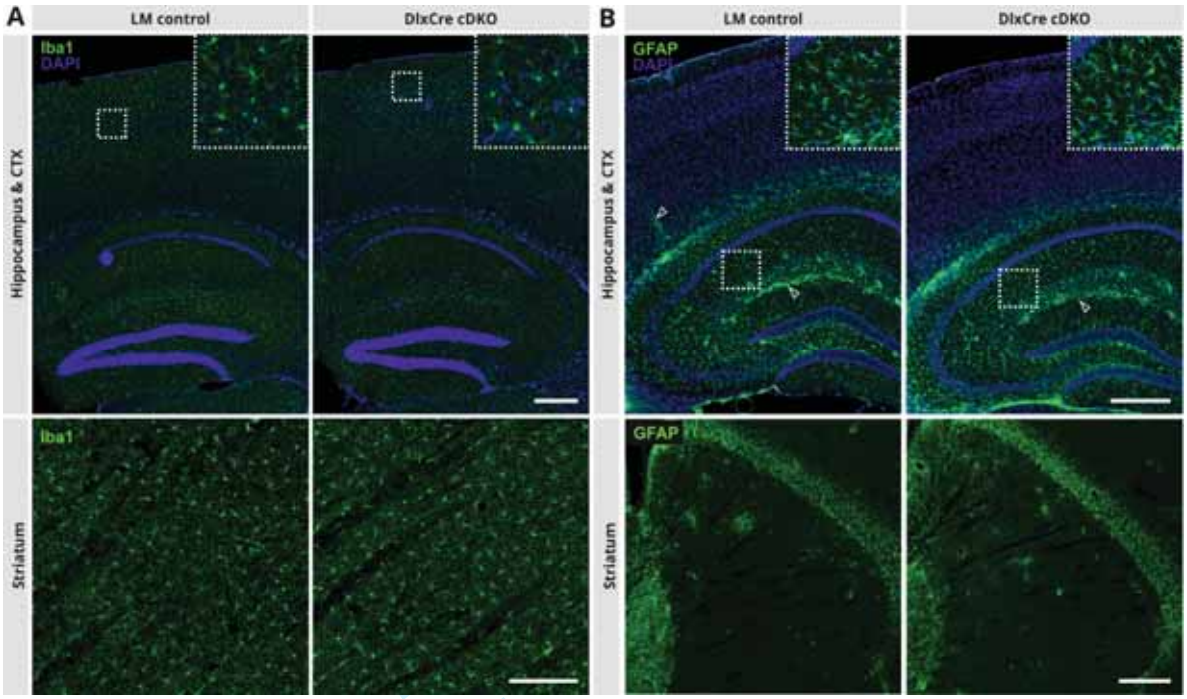

Figure S10